Inorg. Chem. **2006**, *45*, 6161–6178

Theoretical Studies of Phosphorescence Spectra of Tris(2,2′-bipyridine) Transition Metal Compounds

Koichi Nozaki,* Keisei Takamori, Yuji Nakatsugawa, and Takeshi Ohno

Department of Chemistry, Graduate School of Science, Osaka University, 1-16 Machikaneyama, Toyonaka, Osaka 560-0043, Japan

Received December 1, 2005

Phosphorescence spectra of tris(2,2′-bipyridine) metal compounds, $[M(bpy)_3]^{n+}$, where M = Zn(II), Ru(II), Os(II), Rh(III), and Ir(III), were calculated using a harmonic oscillator approximation of adiabatic potential surfaces obtained by density functional theory (DFT). Using the Huang–Rhys (S) factors calculated by theoretical Franck–Condon analysis of T_1 and S_0 geometries, we successfully reproduced the emission spectra observed under various conditions by nonempirical calculations. The simulations of well-structured spectra of the Zn(II), Rh(III), and Ir(III) compounds confirmed that the emission originated from localized ligand-centered excited states with considerably distorted geometries of C_2 symmetry. The spectrum simulation revealed that the phosphorescence state of $[Ru(bpy)_3]^{2+}$ was localized ^{3}MLCT both in a solution and a glass matrix. Furthermore, a highly resolved phosphorescence spectrum observed for $[Ru(bpy)_3]^{2+}$ doped in a $[Zn(bpy)_3](ClO_4)_2$ crystal was reproduced well using the geometry of the localized ^{3}MLCT by assuming mode-specific broadening of low-frequency intramolecular vibrational modes. The deuterium effects of the electronic origins of the doped crystal observed by Riesen et al. were in excellent agreement with those predicted for the localized ^{3}MLCT. However, the calculated satellite structures of the localized ^{3}MLCT involving bpy-h_8 in $[Ru(bpy\text{-}h_8)_{3-x}(bpy\text{-}d_8)_x]^{2+}$ (x = 1,2) exhibited only the bpy-h_8 vibrational modes, inconsistent with the simultaneous appearance of both bpy-h_8 and bpy-h_8 modes in the observed spectra. A simulation on the basis of the geometry of the delocalized ^{3}MLCT was in reasonable agreement with an unresolved spectrum observed for a neat crystal of $[Ru(bpy)_3](PF_6)_2$, which is inconsistent with the assignments of localized ^{3}MLCT on the basis of the electronic origins. The inconsistency of the assignment on the basis of the adiabatic model is discussed in terms of vibronic coupling between the localized ^{3}MLCT states. The ^{3}MLCT state in $[Os(bpy)_3]^{2+}$ seems to vary with the environment: a fully localized ^{3}MLCT in a solution, partially localized in a glass matrix, and delocalized in PF_6 salts.

Introduction

Increasing attention has been paid to transition metal compounds exhibiting intense metal-to-ligand charge transfer (MLCT) phosphorescence for developing organic light emitting diodes (OLED) with high current-to-light conversion efficiency.[1−3] The MLCT phosphorescence of these compounds is characterized by a large radiative rate constant ($\sim 1 \times 10^6\ s^{-1}$)[4] and such large rates enable high-current operation with minimal degradation due to T−T annihilation.[5,6] The strong phosphorescence of these compounds originates from intensity-borrowing of the transition dipole moments of singlet excited states via spin−orbit interaction. Theoretical calculations including spin−orbit coupling have been attempted in an effort to understand the photophysical proper-

* To whom correspondence should be addressed. E-mail: nozaki@ch.wani.osaka-u.ac.jp.

(1) (a) Baldo, M. A.; Lamansky, S.; Burrows, P. E.; Thompson, M. E.; Forrest, S. R. *Appl. Phys. Lett.* **1999**, *75*, 4. (b) Adachi, C.; Baldo, M. A.; Thompson, M. E.; Forrest, S. R. *J. Appl. Phys.* **2001**, *90*, 5048. (c) O'Brien, D. F.; Baldo, M. A.; Thompson, M. E.; Forrest, S. R. *Appl. Phys. Lett.* **1999**, *74*, 442.

(2) Lamansky, S.; Djurovich, P.; Murphy, D.; Abdel-Razzaq, F.; Lee, H.-E.; Adachi, C.; Burrows, P. E.; Forrest, S. R.; Thompson, M. E. *J. Am. Chem. Soc.* **2001**, *123*, 4304.

(3) Nazeeruddin, M. K.; Humphry-Baker, R.; Berner, D.; Rivier, S.; Zuppiroli, L.; Grätzel, M. *J. Am. Chem. Soc.* **2003**, *125*, 8790.

(4) Tsuboyama, A.; Iwawaki, H.; Furugori, M.; Mukaide, T.; Kamatani, J.; Igawa, S.; Moriyama, T.; Miura, S.; Takiguchi, T.; Okada, S.; Hoshino, M.; Ueno, K. *J. Am. Chem. Soc.* **2003**, *125*, 12971.

(5) (a) Adachi, C.; Baldo, M. A.; Forrest, S. R. *J. Appl. Phys.* **2000**, *87*, 8049. (b) Baldo, M. A.; Thompson, M. E.; Forrest, S. R. *Nature* **2000**, *403*, 750. (c) Adachi, C.; Baldo, M. A.; Forrest, S. R.; Lamansky, S.; Thompson, M. E.; Kwong, R. C. *Appl. Phys. Lett.* **2001**, *78*, 1622.

(6) Wang, Y.; Herron, N.; Grushin, V. V.; LeCloux, D.; Petrov, V. *Appl. Phys. Lett.* **2001**, *79*, 449.

10.1021/ic052068r CCC: $33.50
Published on Web 07/04/2006

ties of transition metal compounds, such as zero-field splittings and radiative rates of phosphorescence.[7−12]

For the lowest excited state of highly symmetric tris-chelate metal compounds, two limiting electronic configurations have been proposed: excited state delocalized over three metal−ligand subunits and that localized on a single metal−ligand subunit. The localization involves lowering the symmetry of the excited-state structure with considerable geometrical distortion and then influencing its photophysical properties as demonstrated for $[Ru(bpy)_3]^{2+}$ or $[Os(bpy)_3]^{2+}$.[7−9] The phosphorescence states of Ru(II) and Os(II) diimine compounds are known to exhibit the ^{3}MLCT characteristics, and it has been argued for a long time whether the excited state in $[Ru(bpy)_3]^{2+}$ is localized. For ^{3}MLCT states in a solution or glass matrix, time-resolved resonance Raman[13,14] and transient infrared experiments[15] support the localization models. Furthermore, solvatochromism[16] or Stark effects of the MLCT absorption band of $[Ru(bpy)_3]^{2+}$ indicate that ^{1}MLCT has a considerable dipole moment of ca. 10 D,[17] suggesting that the promoted electron is localized spontaneously or is due to solute−solvent dipolar interaction in MLCT. Also, for the luminescence in a doped crystal, the dipole moment of ^{3}MLCT is estimated to be 1.2 e Å (= 5.8 D) from a large Stark effect,[18] indicating the localization of the promoted electron. Zeeman,[18,19] MCPL,[20] and hole-burning measurements[21] supported the assignment that ^{3}MLCT is localized in single crystals; however, the electronic configuration in the single crystals is still under debate.[22,23] The main point in the dispute is the deuterium effects of the electronic origin in a partially deuterated compound $[Ru(bpy\text{-}h_8)_{3-x}(bpy\text{-}d_8)_x]^{2+}$ ($x = 1$ or 2).[21,23−26] The delocalized model supports one single origin, whereas two origins corresponding to ^{3}MLCT involving bpy-h_8 and bpy-d_8 should appear according to the localized model. Riesen et al. observed two sets of origins for the compounds for $[Ru(bpy)_3]^{2+}$ doped into a $[Zn(bpy)_3](ClO_4)_2$ crystal,[21,24,25] whereas it was claimed by Yersin et al. that they could observe one set of origin in a similar condition.[26] Two sets of origins were observed by Riesen et al. also for the partially deuterated compound in a neat PF_6 salt.[24b,24c] The independent ^{3}MLCT transitions to bpy and bpy-d_2 were clearly shown in $[Ru(bpy)(bpy\text{-}d_2)_2]^{2+}$.[24c] The simultaneous appearance of both bpy-h_8 and bpy-d_8 modes in highly resolved spectra for the partially deuterated compounds is also involved in the dispute.[22,24,27] The pattern with equally strong satellites for both bpy-h_8 and bpy-d_8 modes is likely to support the delocalized model, though it can be interpreted in terms of electronic interaction through the metal center.[23,24] Riesen et al. showed that the simultaneous appearance does not support delocalization because they observed satellites that can be assigned to bpy modes in the luminescence spectra for $[Ru(bpy)_2(bpz)]^{2+}$, in which ^{3}MLCT is localized on the bpz ligand.[24a,28]

In this work, the phosphorescence spectra of $[M(bpy)_3]^{n+}$, M = Zn(II), Ru(II), Os(II), Rh(III), Ir(III), have been studied theoretically. The compounds of Ru(II) and Os(II) show MLCT phosphorescence, whereas the other compounds exhibit emission from a ligand-centered excited state (LC). The vibrational structures for allowed transitions are mainly determined by Franck−Condon progressions that result from overlap integrals of vibrational wave functions between the excited and ground states. Thus, emission spectra can be simulated from the geometrical parameters determined for both emitting and ground states. Because the vibrational structure is very sensitive to geometrical changes upon optical transition, the calculations of electronic spectra in combination with highly accurate quantum chemistry have been employed to determine excited-state structures, such as anthracence, oligophenylenevinylenes, thiophene oligomers, and silicon phthalocyanine.[29−42] This work demonstrates that not only unresolved emission spectra of fluid or glassy solutions but also highly resolved emission spectra of single crystals can be successfully reproduced using a crude adiabatic approximation of vibronic states and the geometries

(7) Kober, E. M.; Meyer, T. J. *Inorg. Chem.* **1982**, *21*, 3967.
(8) Ferguson, J.; Herren, F. *Chem. Phys.* **1983**, *76*, 45.
(9) Kober, E. M.; Meyer, T. J. *Inorg. Chem.* **1984**, *23*, 3877.
(10) Daul, C.; Baerends, E. J.; Vernooijs, P. *Inorg. Chem.* **1994**, *33*, 3538.
(11) (a) Siddique, Z. A.; Yamamoto, Y.; Ohno, T.; Nozaki, K. *Inorg. Chem.* **2003**, *42*, 6366. (b) Siddique, Z. A.; Ohno, T.; Nozaki, K.; Tsubomura, T. *Inorg. Chem.* **2004**, *43*, 663.
(12) Nozaki, K. *J. Chin. Chem. Soc.* **2006**, *53*, 101.
(13) Dallinger, R. F.; Woodruff, W. H. *J. Am. Chem. Soc.* **1979**, *101*, 4391.
(14) Bradley, P. G.; Kress, N.; Hornberger, B. A.; Dallinger, R. F.; Woodruff, W. H. *J. Am. Chem. Soc.* **1981**, *103*, 7441.
(15) Omberg, K. M.; Schoonover, J. R.; Tredway, J. A.; Leasure, R. M.; Dyer, R. B.; Meyer, T. J. *J. Am. Chem. Soc.* **1997**, *119*, 7013.
(16) Chen, P.; Meyer, T. J. *Chem. Rev.* **1998**, *98*, 1439.
(17) (a) Oh, D. H.; Boxer, S. G. *J. Am. Chem. Soc.* **1989**, *111*, 1130. (b) Karki, L.; Hupp, J. T. *Inorg. Chem.* **1997**, 36, 3318. (c) Kober, E. M.; Sullivan, B. P.; Meyer, T. J. *Inorg. Chem.* **1984**, *23*, 2098.
(18) Riesen, H.; Rae, A. D.; Krausz, E. *J. Lumin.* **1994**, *62*, 123.
(19) Riesen, H.; Krausz, E. *Chem. Phys. Lett.* **1994**, *217*, 613.
(20) Riesen, H.; Krausz, E. *Chem. Phys. Lett.* **1988**, *151*, 71.
(21) Riesen, H.; Wallace, L.; Krausz, E. *Inorg. Chem.* **2000**, *39*, 5044.
(22) Yersin, H.; Humbs, W. *Inorg. Chem.* **1999**, *38*, 5820.
(23) Riesen, H.; Wallace, L.; Krausz, E. *Int. Rev. Phys. Chem.* **1997**, *16*, 291.
(24) (a) Riesen, H.; Wallace, L.; Krausz, E. *Chem. Phys.* **1995**, *198*, 269. (b) Riesen, H.; Krausz, E.; Puza, M. *Chem. Phys. Lett.* **1988**, *151*, 65. (c) Riesen, H.; Wallace, L.; Krausz, E. *J. Phys. Chem.* **1996**, *100*, 17138.
(25) (a) Riesen, H.; Krausz, E. *J. Chem. Phys.* **1993**, *99*, 7614. (b) Riesen, H.; Wallace, L.; Krausz, E. *J. Phys. Chem.* **1995**, *99*, 16808.
(26) Yersin, H.; Humbs, W.; Strasser, J. *Top. Curr. Chem.* **1997**, *191*, 153.
(27) Braun, D.; Huber, P.; Wudy, J.; Schmidt, J.; Yersin, H. *J. Phys. Chem.* **1994**, *98*, 8044.
(28) Riesen, H.; Wallace, L.; Krausz, E. *J. Phys. Chem.* **1996**, *100*, 4390.
(29) Zgierski, Z. *Chem. Phys.* **1986**, *108*, 61.
(30) Sharp, T. E.; Rosenstock, H. M. *J. Chem. Phys.* **1964**, *41*, 3453.
(31) Kupka, H.; Cribb, P. H. *J. Chem. Phys.* **1986**, *85*, 1303.
(32) Chen, P. In *Unimolecular and Biomolecular Ion−Molecule Reaction Dynamics*; Ng, C. Y., Baer, T., Powis, I., Eds.; Wiley: Chichester, U.K., 1994.
(33) Yamaguchi, M.; Momose, T.; Shida, T. *J. Chem. Phys.* **1990**, *93*, 4211, **1990**, *93*, 4223.
(34) Takahashi, J.; Momose, T.; Shida, T. *Bull. Chem. Soc. Jpn.* **1994**, *67*, 964.
(35) Siebrand, W.; Zerbetto, F.; Zgierski, Z. *J. Phys. Chem.* **1989**, *91*, 5926.
(36) Chau, F.; Dyke, J. M.; Lee, E. P.; Wang, D. *J. Electron Spectrosc.* **1998**, *97*, 33.
(37) Hemley, R. J.; Lasaga, A. C.; Vaida, V.; Karplus, M. *J. Phys. Chem.* **1988**, *92*, 945.
(38) Zerbetto, F.; Zgierski, Z. *Chem. Phys.* **1988**, *127*, 17.
(39) Dierksen, M.; Grimme, S. *J. Chem. Phys.* **2004**, *120*, 3544.
(40) (a) Gierschner, J.; Mack, H.-G.; Oelkrug, D.; Waldner, I.; Rau, H. *J. Phys. Chem. A* **2004**, *108*, 257. (b) Gierschner, J.; Mack, H.-G.; Lüer, L.; Oelkrug, D. *J. Chem. Phys.* **2002**, *116*, 8596.
(41) Negri, F.; Zgierski, M. *J. Chem. Phys.* **1994**, *100*, 2571.
(42) Braun, D.; Titeca, B. C.; Ceulemans, A. *J. Porphyrins Phthalocyanines* **2001**, *5*, 33.

obtained by density functional theory (DFT). Geometrical changes in the excited states of the metal compounds were then determined. It is also revealed that the simulation based on a crude adiabatic approximation could not give consistent assignments of the electronic configuration of ^{3}MLCT in $[Ru(bpy)_3]^{2+}$. Vibronic couplings responsible for the inconsistency are discussed.

Experimental Section

(I) Materials. $[Zn(bpy)_3](PF_6)_2$,[43] $[Rh(bpy)_3](PF_6)_2$,[44] $[Ru(bpy)_3](PF_6)_2$,[45] and $[Os(bpy)_3](PF_6)_2$[46] were synthesized according to methods published in the literature.

(II) Instrumentation. Steady-state emission spectra were recorded using a grating monochromator (Triax 1900) with a CCD image sensor (Hamamatsu S7031). The spectral sensitivity of the spectrofluorometer was corrected using a bromine lamp (Ushio IPD 100V 500WCS). A sample in a 2 mm diameter cylindrical quartz cell was excited using an argon ion laser (488 nm, 100 mW, INNOVA 300 Coherent Co.) or Nd^{3+}:YAG laser (355 nm, 2mW, NANOLASE). The spectra at 77 K were measured using a liquid-nitrogen Dewar. For the measurement of the phosphorescence from $[Zn(bpy)_3](PF_6)_2$, a sample solution was excited with a high-pressure mercury lamp at 314 nm and the fluorescence component was blocked using a rotating sector. The emission intensity in all the spectra is relative to quanta at each frequency.

(III) Computational Chemistry. Density functional calculations were carried out with GAUSSIAN 98, Rev A11.3 (G98) and GAUSSIAN 03, Rev C02 (G03).[47] Several basis functions were used for the calculation. LANL2DZ is the Dunning−Hay split valence double-ζ for C,H,N atoms (D95) and Hay−Wadt double-ζ with Los Alamos relativistic effective core potential for heavy atoms.[48] For comparison, D95 plus one polarization function (D95*) or Pople's split valence double-ζ basis sets with one polarization function (6-31G(d,p))[49] were used for C, H, N atoms. As a pure density functional, the Perdew−Wang exchange-correlation (PW91PW91)[50] was used. As a hybrid DFT, Becke's style three-parameter hybrid functional was defined as

$$E_{xc}^{B3} = (1-a)E_x^{LSDA} + aE_x^{exact} + b\Delta E_x^{B88} + E_c^{LSDA} + c\Delta E_c^{GGA} \quad (1)$$

a linear combination of Hartree−Fock (exact) exchange term with a local exchange functional of Slater and a local spin density approximation with VWN,[51] nonlocal exchange proposed by Becke, and a generalized gradient approximated (GGA) correlation functional of Perdew and Wang, PW91 (B3PW91)[50] or LYP(B3LYP).[52] The parameters a, b, and c are determined by fitting to experimental data of selected molecules: $a = 0.20$, $b = 0.72$, and $c = 0.81$.[53] The integration grid used for two-electron integrals was a fine pruned (75,302) grid, whereas geometry optimizations, calculations of excited-state properties, and frequency analyses for the compounds of the D_3 point group were calculated using an ultrafine pruned (99,590) grid.

The geometries of the lowest triplet states were calculated at an unrestricted DFT level with a spin multiplicity of 3, e.g., UB3PW91. For calculation with difficulty in the SCF convergence, a quadratically convergent (QC) SCF procedure[54] was used instead of Pulay's direct inversion in the iterative subspace extrapolation method (DIIS).[55] The effects of solvation on electronic structures were simulated using an Onsager model,[56] which considered the electrostatic interaction of solvation energy for a spherical solute with a dipole immersed in a dielectric continuum. Normal vibrational mode analysis was performed at the B3PW91/LANL2DZ level. Deuterium effects in zero-point energy (ZPE) for the excited states in the Rh(III) and Ru(II) compounds were calculated at the (U)-B3PW91/LANL2DZ level. To obtain the zero point energies with high precision ($\sim$1 cm^{-1}), normal vibrational mode analysis was performed using an ultra fine grid (99,590) for the geometries obtained with extremely tight convergence criteria (very tight being the key word). The scaling factor of 0.9521 determined for 42 organometallic compounds at the B3LYP/LANL2DZ level was used for all cases.[57]

All quantum chemical calculations were carried out on a lab-developed PC cluster system consisting of 30 Pentium IV CPUs (2.5−3 GHz) and 16 Athlon MP CPUs (1800+, 2400+). The calculations of Huang−Rhys factors, solvent reorganization energies, and emission spectra were performed using lab-developed programs.

Theory

1. Calculation of Huang−Rhys (S) Factors for Vertical Transition. The Franck−Condon state produced in a vertical transition between two potential surfaces such as the radiative process (point f, Figure 1) has a structure in which each atom is displaced from the stationary point of the ground state (point p). Because the structure of the Franck−Condon state is identical to that of the stationary point of the excited-state potential surface (point r), a displacement vector (Δx) is defined from the differences in Cartesian coordinates between the structures optimized for the ground and excited states (r and p) (eq 2).

$$\Delta x = (x_{1p} - x_{1r}, y_{1p} - y_{1r}, z_{1p} - z_{1r}, \ldots, x_{Np} - x_{Nr}, y_{Np} - y_{Nr}, z_{Np} - z_{Nr})^T \quad (2)$$

The projection of the displacement vector to $3N - 6$ normal

(43) Ohno, T.; Kato, S. *Bull. Chem. Soc. Jpn.* **1974**, *47*, 2953.
(44) Harris, C. M.; McKenzie, E. D. *J. Inorg. Nucl. Chem.* **1963**, *25*, 171.
(45) Palmer, R. A.; Piper, T. S. *Inorg. Chem.* **1966**, *5*, 864.
(46) Burstall, F. J.; Dwyer, F. P.; Gyartus, E. C. *J. Chem. Soc.* **1950**, 953.
(47) Frisch, M. J.; Trucks, G. W.; Schlegel, H. B.; Scuseria, G. E.; Robb, M. A.; Cheeseman, J. R.; Zakrzewski, V. G.; Montgomery, J. A.; Stratmann, R. E.; Burant, J. C.; Dapprich, S.; Millam, J. M.; Daniels, A. D.; Kudin, K. N.; Strain, M. C.; Farkas, O.; Tomasi, J.; Barone, V.; Cossi, M.; Cammi, R.; Mennucci, B.; Pomelli, C.; Adamo, C.; Clifford, S.; Ochterski, J.; Petersson, G. A.; Ayala, P. Y.; Cui, Q.; Morokuma, K.; Malick, D. K.; Rabuck, A. D.; Raghavachari, K.; Foresman, J. B.; Cioslowski, J.; Ortiz, J. V.; Stefanov, B. B.; Liu, G.; Liashenko, A.; Piskorz, P.; Komaromi, I.; Gomperts, R.; Martin, R. L.; Fox, D. J.; Keith, T.; Al-Laham, M. A.; Peng, C. Y.; Nanayakkara, A.; Gonzalez, C.; Challacombe, M.; Gill, P. M. W.; Johnson, B. G.; Chen, W.; Wong, M. W.; Andres, J. L.; Head-Gordon, M.; Replogle, E. S.; Pople, J. A. *Gaussian 98*, revision A.11.3; Gaussian Inc.: Pittsburgh, PA, 1998.
(48) (a) Dunning, T. H., Jr.; Hay, P. J. In *Modern Theoretical Chemistry*; Schaefer, H. F., III, Ed.; Plenum: New York, 1976; Vol. 3. (b) Hay, P. J.; Wadt, W. R. *J. Chem. Phys.* **1985**, *82*, 270. Hay, P. J.; Wadt, W. R. *J. Chem. Phys.* **1985**, *82*, 284. Hay, P. J.; Wadt, W. R. *J. Chem. Phys.* **1985**, *82*, 299.
(49) Ditchfield, R.; Hehre, W. J.; Pople, J. A. *J. Chem. Phys.* **1971**, *54*, 724.
(50) (a) Perdew, J. P. *Phys. Rev. B* **1986**, *33*, 8822. (b) Perdew, J. P.; Burke, K.; Wang, Y. *Phys. Rev. B* **1996**, *54*, 16533.
(51) Vosko, S. H.; Wilk, L.; Nusair, M. *Can. J. Phys.* **1980**, *58*, 1200.
(52) Lee, C.; Yang, W.; Parr, P. G. *Phys. Rev. B* **1988**, *37*, 785.
(53) Becke, A. D. *J. Chem. Phys.* **1993**, *98*, 5648.
(54) Bacskay, G. B. *Chem. Phys.* **1981**, *61*, 385.
(55) Pulay, P. *J. Comput. Chem.* **1982**, *3*, 556.

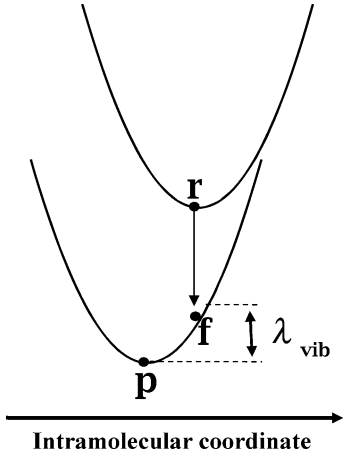

Figure 1. Vertical transition from the bottom of the excited state (r) produces the Franck−Condon state (f), which is displaced from the stationary point of the ground state (p). The energy difference between p and f on the potential curve denotes vibrational reorganization energy (λ_{vib}) associated with vertical transition.

vibrational coordinates of the ground state gives the Huang−Rhys factors (S) for the vertical transition.

The normal vibrational coordinates, Q, and their vibrational frequencies, ω, of a given molecule are obtained from the diagonalization of a Hessian matrix scaled by the mass of each atom, F^{mxx} ($= m^{-1/2}F^{xx}m^{-1/2}$), where the Hessian matrix, F^{xx}, is the second derivative of potential energy with respect to the Cartesian coordinate (eq 3).[30,32,34b,37,40]

$$\Lambda = L_{mx}^{T} F^{mxx} L_{mx} \tag{3}$$

$$\Delta Q = L_{mx}^{T} m^{1/2} \Delta x = L_{mx}^{T} \Delta x_m \tag{4}$$

where Λ is a diagonal matrix with the elements being $4\pi^2\omega^2$ and $m^{1/2}$ is a diagonal matrix with the elements being square roots of each atom. L_{mx} is a transform matrix from the normal vibrational coordinate ΔQ and mass-weighted displacement vector in the Cartesian coordinate, Δx_m. Using eq 4, the displacement vector is readily transformed to the displacement vector with respect to the normal vibrational coordinate. The vibrational reorganization energy is obtained as the sum of the potential energies along with normal vibrational coordinates, namely mode-specific reorganization energy $\lambda_{vib,i}$ (eq 5).

$$\lambda_{vib} = \sum_{i}^{3N-6} \lambda_{vib,i} = \sum_{i}^{3N-6} 2\pi^2 \omega_i^2 \Delta Q_i^2 \tag{5}$$

The projection of the displacement vector using eq 4 does not always succeed. In molecules with internal rotational freedoms, rotational displacement sometimes tends to be transformed to displacement in vibrational modes and causes an unusually large λ_{vib}. The erroneous projection is readily identified by checking whether λ_{vib} is equal to the difference in SCF energy between the structures at p and at f.

Finally, the Huang−Rhys factor for the i-th normal vibrational mode is given by eq 6.

$$S_i = \frac{2\pi^2 \omega_i \Delta Q_i^2}{\hbar} \tag{6}$$

In the calculation of the displacement vector Δx, the alignment of the excited-state geometry must be carefully adjusted to that of the ground state. Although any displacement vectors for translation of the molecule are orthogonal to all normal vibrational vectors, the displacement vectors for rotation are orthogonal only when the displacement is very small. Large rotational displacement inevitably causes serious errors in calculating Huang−Rhys factors of vibrations. Therefore, the rotational displacement of the excited-state molecule must be minimized prior to the calculation of Δx. Vectors for rotation around the x, y, and z axes are defined as follows

$$\begin{aligned} R_x &= m^{1/2}(0, z_1, -y_1, 0, z_2, -y_2, \ldots, 0, z_N, -y_N)^T \\ R_y &= m^{1/2}(z_1, 0, -x_1, z_2, 0, -x_2, \ldots, z_N, 0, -x_N)^T \\ R_z &= m^{1/2}(y_1, -x_1, 0, y_2, -x_2, 0, \ldots, y_N, -x_N, 0)^T \end{aligned} \tag{7}$$

where x_j, y_j, and z_j denote the coordinates of the j-th atom relative to the gravity of the molecule. These rotational vectors are orthogonal to column vectors in L_{mx}. The orientation of the excited-state geometry was adjusted so that all three products, $\Delta x_m R_x$, $\Delta x_m R_y$, and $\Delta x_m R_z$, approached zero.

In this work, vibrational frequencies ω and the transform matrix L_x ($= m^{-1/2}L_{mx}$) were obtained from frequency analysis at the B3PW91/LANL2DZ level for ground-state molecules using the G98 program suite. Because the change in zero-point energy between the ground and excited states is less than 1% for these compounds, vibrational frequencies and normal vibrational coordinates are assumed to be invariant in the determination of S factors.

2. Calculation of Solvent Reorganization Energy Involved in a Vertical Transition. When the charge distribution on a molecule changes in association with electronic transition, the coupling of the electronic transition with the orientational or electric polarization of the solvent causes a broadening and shift of electronic spectra.[58] The solvent reorganization energy λ_s is defined as the difference in solvation energy between the Franck−Condon state (f) and the fully relaxed state (p) in Figure 2. Solvation energies at points p and r result from electrostatic interaction between the charge on the solute and the slow component of solvent polarization ϵ_s. On the other hand, for solvation at point f, only electric polarization follows the change in charge distribution because orientational polarization is frozen during

(56) (a) Onsager, L. *J. Am. Chem. Soc.* **1936**, *58*, 1486. (b) Wong, M. W.; Frisch, M. J.; Wiberg, K. B. *J. Am. Chem. Soc.* **1991**, *113*, 4776. Wong, M. W.; Frisch, M. J.; Wiberg, K. B. *J. Am. Chem. Soc.* **1992**, *114*, 523. Wong, M. W.; Frisch, M. J.; Wiberg, K. B. *J. Am. Chem. Soc.* **1992**, *114*, 1645.

(57) Yu, L.; Sriniras, G. N.; Schwartz, M. *J. Mol. Struct. (THEOCHEM)* **2003**, *625*, 215.

(58) (a) Marcus, R. A. *J. Chem. Phys.* **1965**, *43*, 679. (b) Marcus, R. A. *J. Phys. Chem.* **1994**, *98*, 7170. (c) Liu, Y.-P.; Newton, M. D. *J. Phys. Chem.* **1995**, *99*, 12382.

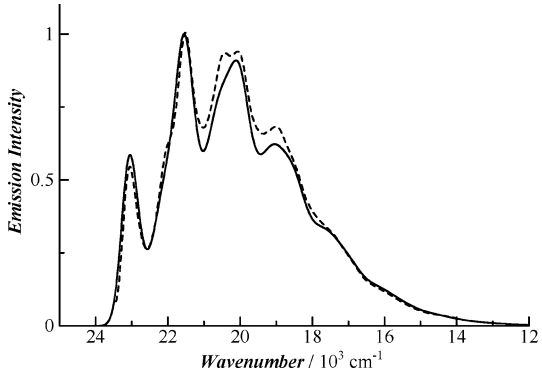

Figure 2. Experimental and calculated phosphorescence spectra for $[Zn(bpy)_3]^{2+}$. Dashed lines, observed in a butyronitrile glass at 77 K; solid line, calculated from eqs 10−12 using the *S* factors obtained for the B3PW91/LANL2DZ geometries, $n_{inh} = 450\ cm^{-1}$, $\nu_{00} = 23.15 \times 10^3\ cm^{-1}$, $T = 77$ K, and $\lambda_s = 0$.

vertical transition. Therefore, the solvent reorganization energy is approximately given by eq 8.[59]

$$\lambda_s \approx (E_{es}[\rho_r(r),\epsilon_s] + E_{es}[\rho_r(r) - \rho_f(r),\epsilon_{op}]) - E_{es}[\rho_p(r),\epsilon_s] \quad (8)$$

where $\rho_p(r)$ and $\rho_r(r)$ represent the charge distribution on the solute at points r and p, respectively, and $E_{es}[\rho(r),\epsilon]$ denotes solute−solvent interaction energy and polarization energy when a solute with $\rho(r)$ is immersed in a dielectric continuum with ϵ. ϵ_{op} is the infinite response component of the dielectric constant. Assuming the linear response of the solvent polarization and ignoring the polarizability of the solute, namely, $\rho_f(r) \approx \rho_p(r)$, eq 8 is approximated by eq 9.

$$\lambda_s \approx E_{es}[\Delta\rho(r),\epsilon_{op}] - E_{es}[\Delta\rho(r),\epsilon_s] \quad (9)$$

where $\Delta\rho(r) = \rho_r(r) - \rho_p(r)$.

The electrostatic portion of solvation was calculated using Tomasi's polarizable continuum model (PCM),[60] in which the solute in a cavity is immersed in a dielectric continuum and the reaction potential is considered to arise from surface charge densities on the cavity. The cavity employed in this work was a solvent-excluded surface (SES), formed by fused spheres centered on solute atoms according to the GEPOL93 algorithm.[61] The atomic radii used for forming the cavity were Pauling's atomic radii with a scaling factor of 1.2: 1.44 Å (H), 1.80 Å (C), and 1.80 Å (N).[62] The radii of the heavy atoms (Ru, Os, Ir) were set to 2.0 Å. The solvent molecules of acetonitrile and dichloromethane were approximated by spheres with radii of 2.1 and 2.2 Å, respectively.[63] The change in the charge distribution on the solute $\Delta\rho(r)$ was approximated as being the difference in the Mulliken charge on each atom. Atomic charges on hydrogen atoms were summed into the connecting heavy atoms. The dielectric constant inside the cavity was assumed to be 1.

3. Calculation of Emission Spectrum. The representation of an emission spectrum using time-dependent formalism was developed by Mukamel et al.[64]

$$I(\nu_{em}) \propto \nu_{em}{}^3 \mathrm{Re}[\int dt \exp[i(\nu_{em} - \nu_{00})t - g(t)] \prod_{j=1}^{3N-6} \sigma_j(t)] \quad (10)$$

$$g(t) = \left(\frac{\pi^2 \Delta\nu_{inh}{}^2}{4 \ln 2} + \frac{\lambda_s}{\beta\hbar^2}\right)t^2 + i\frac{\lambda_s}{\hbar}t \quad (11)$$

where $\Delta\nu_{inh}$ is full width at half-maximum due to inhomogeneous broadening and λ_s is the solvent reorganization energy. Re means the real part of a complex number. When emission arises from thermally equilibrated vibrational states at temperature *T*, the time domain representation of the Franck−Condon progression of mode *j*, $\sigma_j(t)$, is given by eq 12, assuming that both the change in vibrational frequency and mixing of normal vibrational modes are ignored

$$\sigma_j(t) = \exp\left(S_j \frac{\exp(-i\omega_j t) - 1 + \exp(-\beta\hbar\omega_j)[\exp(i\omega_j t) - 1]}{1 - \exp(-\beta\hbar\omega_j)}\right) \quad (12)$$

where $\beta = (kT)^{-1}$.

In the calculation of spectra using eqs 10−12, the number of data points was 4096 for low-resolution emission spectra and 16 384 for highly resolved ones. The energy interval in the spectrum simulation was ca. 4 cm^{-1} for the former and 0.2 cm^{-1} for the latter. The effect of specific broadening of a mode with ω_j and S_j was simulated by replacing it by multiple modes centered at ω_j in calculating $\sigma_j(t)$. The *S* values for multiple modes were determined so that the profile of *S* vs ω is Gaussian-shaped and their sum equals S_j.

Results and Discussion

Geometries at the Ground State (S_0). The geometries of the tris-chelate metal compounds were obtained with the automatic geometry optimization procedure in the G98 program suite. The optimized structures for the bpy compounds belonged to the D_3 point group. The resulting geometries were dependent on the density functionals and the basis functions employed. Table 1 shows the selected bond lengths for the ground-state geometries at various combinations of density functionals and basis functions. The use of the well-known B3LYP functional and Pople's split-valence double-ζ functions (i.e., the B3LYP/(6-31G(d,p) +LANL2DZ)) was found to give slightly longer (10−30 mÅ) metal-to-nitrogen bond lengths than experimental lengths. In particular, the metal-to-nitrogen distance in $[Ru(bpy)_3]^{2+}$ was difficult to reproduce using the B3LYP functional. In the geometries optimized at the B3PW91/(D95+LANL2DZ) (= B3PW91/LANL2DZ) level, although

(59) Bonaccorsi, R.; Cimiraglia, R.; Tomasi, J. *Chem. Phys. Lett.* **1983**, *99*, 77.
(60) (a) Miertus, S.; Scrocco, E.; Tomasi, J. *Chem. Phys.* **1981**, *55*, 117. (b) Bonaccorsi, R.; Palla, P.; Tomasi, J. *J. Am. Chem. Soc.* **1984**, *106*, 1945. (c) Cammi, R.; Tomasi, J. *J. Chem. Phys.* **1994**, *100*, 7495.
(61) Pascual-Ahuir, J. L.; Silla, E.; Tunon, I. *J. Comput. Chem.* **1994**, *15*, 1127.
(62) (a) Weast, R. C. *Handbook of Chemistry and Physics*; CRC Press: Cleveland, OH, 1981. (b) Borone, V.; Cossi, M.; Tomasi, J. *J. Chem. Phys.* **1997**, *107*, 3210.
(63) (a) Weiner, S. J.; Kollman, P. A.; Case, D. A.; Singh, U. C.; Ghio, C.; Alagona, G.; Profeta, S., Jr.; Weiner, P. J. *J. Am. Chem. Soc.* **1984**, *106*, 765. (b) Tawa, G. J.; Martin, R. L.; Pratt, L. R.; Russo, T. V. *J. Phys. Chem.* **1996**, *100*, 1515.
(64) (a) Yan, Y. J.; Mukamel, S. *J. Chem. Phys.* **1986**, *85*, 5908. (b) Myers, A. B. *Chem. Phys.* **1994**, *180*, 215.

Table 1. Selected Bond Lengths in Ground-State Geometries Calculated with Various Density Functionals (DF) and Basis Functions

	basis function		bond distance/Å			
DF	H,C,N	metal	M−N	C(2)−C(2′)	N−C(2)	N−C(6)
			$[Zn(bpy)_3]^{2+}$			
PW91PW91	D95	LANL2DZ	2.210	1.492	1.376	1.364
B3PW91	D95	LANL2DZ	2.200	1.487	1.365	1.354
B3PW91	D95*	LANL2DZ	2.213	1.490	1.351	1.341
B3PW91	6-31G(d,p)	LANL2DZ	2.222	1.487	1.349	1.340
B3LYP	6-31G(d,p)	LANL2DZ	2.237	1.491	1.353	1.343
Exp[65]			2.168	1.476	1.336	1.348
			$[Ru(bpy)_3]^{2+}$			
PW91PW91	D95	LANL2DZ	2.073	1.473	1.390	1.371
B3PW91	D95	LANL2DZ	2.079	1.472	1.375	1.359
B3PW91	D95*	LANL2DZ	2.087	1.475	1.361	1.346
B3PW91	6-31G(d,p)	LANL2DZ	2.094	1.473	1.360	1.344
B3LYP	6-31G(d,p)	LANL2DZ	2.118	1.478	1.364	1.347
Exp[66]			2.056	1.474	1.354	1.354
			$[Os(bpy)_3]^{2+}$			
B3PW91	D95	LANL2DZ	2.068	1.467	1.380	1.364
B3PW91	D95*	LANL2DZ	2.072	1.470	1.365	1.351
B3PW91	6-31G(d,p)	LANL2DZ	2.079	1.467	1.365	1.350
B3LYP	6-31G(d,p)	LANL2DZ	2.077	1.467	1.365	1.350
Exp[67]			2.062	1.470	1.359	1.349

the bond lengths in the ligands were slightly worse than those for the B3PW91/(6-31G(d,p)+LANL2DZ) level, the metal-to-nitrogen bond lengths were the most accurate among the combinations examined here. The lower accuracy in the ligand geometries can be ascribed to the lack of a polarization function in D95 basis sets for carbon and nitrogen atoms. These bond lengths were improved by adding one polarization function to D95 (D95*). Adding one f-type Gaussian function with an exponent of 0.1 to the LANL2DZ basis of metal did not affect the metal-to-nitrogen bond lengths. Judging from the computation cost to the performance ratio, the DFT calculations in this work were performed at the B3PW91/LANL2DZ level. The Cartesian coordinates of the optimized geometry for all the metal compounds are listed in the Supporting Information, Section A.

Simulation of Phosphorescence Spectra. (i) $[Zn(bpy)_3]^{2+}$, $[Rh(bpy)_3]^{3+}$, and $[Ir(bpy)_3]^{3+}$. The geometries at T_1 of the Zn(II), Rh(III), and Ir(III) tris-bpy compounds were optimized at the B3PW91/LANL2DZ level without symmetry constraints. All the resulting structures were found to belong to the C_2 point group, lowered from D_3 at S_0. Because there is no report on the X-ray structures of these compounds in the excited state, the geometrical parameters obtained with the calculations are not evaluated directly. However, the accuracy of the calculation is readily evaluated by examining whether the simulation on the basis of the geometrical parameters for both T_1 and S_0 reproduces the phosphorescence spectrum.

The dashed lines in Figure 2 show the phosphorescence spectrum observed for $[Zn(bpy)_3](ClO_4)_2$ at 77 K in butyronitrile glass. The solid line in Figure 2 indicates the emission simulated using eqs 10−12, with the S factors calculated from the difference in geometry between S_0 and T_1. The parameters adopted in the fitting to the experimental are full width at half-maximum (fwhm) values of inhomogeneous broadening ($\nu_{inh} = 450$ cm^{-1}) and the 0−0 transition energy ($\nu_{00} = 23.15 \times 10^3$ cm^{-1}). Though theoretical modeling of inhomogeneous broadening is difficult, the fwhm of 450 cm^{-1} is not inconsistent with the typical values in a glass matrix (200−500 cm^{-1}). Broadening due to solvent reorganization in eq 11 was ignored in the glass matrix. It is noteworthy that the complicated vibrational structure of the phosphorescence spectrum is almost perfectly reproduced by simulation without empirical parameters. The use of the 6-31G(d,p) basis function instead of D95 caused only slight changes in the spectrum. These results indicate that the geometries obtained at the B3PW91 level are consistent with the observed vibrational progression.

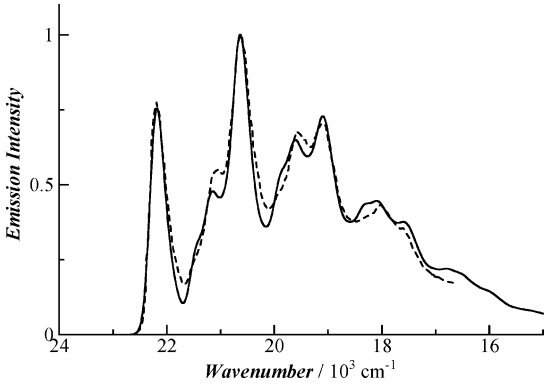

Figure 3. Experimental and calculated phosphorescence spectra for $[Ir(bpy)_3]^{3+}$. Dashed line, observed in a 4:1 EtOH:MeOH glass at 4.2 K (ref 68); solid line, calculated using the S factors for the B3PW91/LANL2DZ geometries, $\nu_{inh} = 270$ cm^{-1}, $\nu_{00} = 22.21 \times 10^3$ cm^{-1}, $T = 4.2$ K, and $\lambda_s = 0$.

Both the phosphorescence spectra of $[Ir(bpy)_3]^{3+}$ (Figure 3, dashed line) and of $[Rh(bpy)_3]^{3+}$ (not shown) exhibit vibrational structures similar to that for $[Zn(bpy)_3]^{2+}$, implying that the T_1 states of these compounds are the $^3\pi\pi^*$ character in bpy. The structures obtained without symmetry constraint for both the Rh(III) and Ir(III) compounds belong to the C_2 point group. The simulated spectra using the calculated S factors are in good agreement with those observed (Figure 3, solid line). The vibrational reorganization energies involved in the phosphorescence of these compounds were evaluated as being 4000 cm^{-1} for $[Zn(bpy)_3]^{2+}$, 3800 cm^{-1} for $[Rh(bpy)_3]^{3+}$, and 3800 cm^{-1} for $[Ir(bpy)_3]^{3+}$.

A single crystal of $[Rh(bpy)_3]^{3+}$ doped into $[Zn(bpy)_3](ClO_4)_2$ at a very low temperature exhibits a highly resolved luminescence spectrum that contains many vibrational satellites corresponding not only to Franck−Condon progressions but also to vibronic coupling.[69] The simulation of such highly resolved spectra is expected to provide more accurate information on the geometry of the emitting state than that of spectra for an amorphous glass or fluid solution. Figure 4 shows the simulated Franck−Condon progressions for $[Rh(bpy)_3]^{3+}$ using the geometrical parameters obtained at the B3PW91/LANL2DZ level with a narrow line width, $\tilde{\nu}_{inh} = 4$ cm^{-1}. Because the simulation using eqs 10−12 does not take into account coupling with lattice modes, the whole shape of the simulated spectrum appears to be different from the reported one. However, most of the vibrational satellites in the observed spectra were reproduced: observed vibrational satellites[70] (calcd) are 179 (152a_1), 208 (175e), 767 (742a_1 + 742e), 1044 (1011a_1), 1053 (1005e), 1329 (1293a_1 + 1293e), 1507 (1473a_1 + 1474e), 1566 (1539a_1 + 1539e),

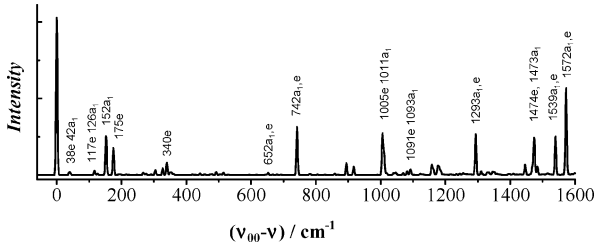

Figure 4. Simulated highly resolved emission spectra for $[Rh(bpy)_3]^{3+}$ at $\nu_{inh} = 4$ cm^{-1} and $T = 1.2$ K.

and 1609 ($1572a_1 + 1572e$) cm $^{-1}$. It is worth noting that two modes, a totally symmetric a_1 and an asymmetric e, in the most-vibrational satellites overlap. The appearance of asymmetric e modes of the ground state in the emission spectrum is ascribed to symmetry-lowering in the excited state. For the internal ligand modes, the trigonal field splitting (frequency difference between a_1 and e modes) is less than 1 cm^{-1}, implying a weak interaction of vibrations among the three bpy ligands in $[Rh(bpy)_3]^{3+}$. Thus, most vibrational satellites corresponding to internal ligand modes consist of two components, not resolved even in narrow-line spectra. The *S* factors of the 1044, 1566, and 1609 modes were estimated to be ca. 0.3 from their intensities relative to the zero-phonon band.[70a] The calculated *S* factors are 0.307 for the 1005e mode, $0.10 + 0.22$ for the $1539a_1 + 1539e$ mode, and $0.25 + 0.47$ for the $1572a_1 + 1572e$ mode. Except for the 1572 mode, the calculated *S* factors are in good agreement with the observed values. The reason for the large *S* factor of the 1572e mode is unclear. The simulated highly resolved spectra of $[Ir(bpy)_3]^{3+}$ and $[Zn(bpy)_3]^{2+}$ are almost the same as those of $[Rh(bpy)_3]^{3+}$.

(ii) $[Ru(bpy)_3]^{2+}$. Calculations of the T_1 geometry for $[Ru(bpy)_3]^{2+}$ were much more difficult, because several excited states with different electronic configurations were similar in energy and the order of these states was strongly dependent on quantum-chemical models, small changes in geometrical parameters, and properties of the surrounding medium. The geometry optimizations for T_1 states in $[Ru(bpy)_3]^{2+}$ and $[Os(bpy)_3]^{2+}$ were performed within the constraints of both D_3 and C_2 symmetry. The calculation under D_3 symmetry yielded the structures corresponding to $^3A_2$ (HOMO(a_1) → LUMO(a_2)) with no dipole moment. The vibrational reorganization (λ_{vib}) for the phosphorescence process of $^3A_2 \rightarrow {}^1A_1$ is calculated to be only 670 cm^{-1} using eq 5. Within the constraints of the lower symmetry of C_2, the optimized structure as the lowest excited state was ^3B (HOMO(a) → LUMO(b)). In addition, the geometry for ^3A (HOMO(a) → LUMO(a)) was also determined as the next-lowest triplet state. Both the states have a non-zero dipole moment.

The effects of polarizability of the surrounding medium were simulated using the Onsager solvation model. In this model, a dipole moment of the solute (μ) in a spherical cavity with a radius of *r* induces polarization of the solvent with a static dielectric constant of ϵ. The polarization in turn forms a reaction field (*R*) on the solute, which interacts with the

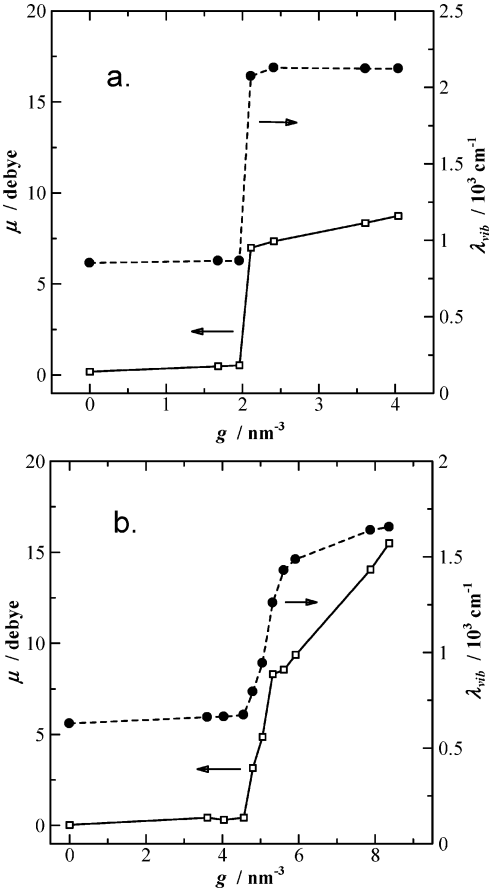

Figure 5. Predicted dipole moment of the T_1 state (open squares) and the vibrational reorganization energy for $T_1 \rightarrow S_0$ (closed circles) as a function of the *g* factors for $[Ru(bpy)_3]^{2+}$ (a) and for $[Os(bpy)_3]^{2+}$ (b). Geometry optimizations for the T_1 states were performed at B3PW91/LANL2DZ under C_2 symmetry constraints.

dipole moment of the solute, leading to electrostatic stabilization of the dipole. The reaction field is given by eq 13.[56b]

$$R = g\mu;\ g = \frac{2(\epsilon - 1)}{(2\epsilon + 1)r^3} \tag{13}$$

Thus, the magnitude of stabilization energy of a polar molecule increases linearly with the *g* factor defined in eq 13. Hereafter, the *g* factor is denoted without its unit (nm^{-3}) in the text for convenience. The geometry of the ^3B state was optimized with various *g* factors, and the dipole moments of the resulting ^3B states of $[Ru(bpy)_3]^{2+}$ are shown as a function of the *g* factors in Figure 5a. For the ^3B state in $[Ru(bpy)_3]^{2+}$, the dipole moments obtained for a *g* factor less than 2.0 were ca. 0.5 D, whereas they steeply increased to about 7.5 D when the *g* factor exceeded 2.0. The direction of the moment vector indicates that the excited electron is localized on a single bpy ligand. The increase in the dipole moment was accompanied by distortion of the structure: the λ_{vib} value for the phosphorescence process of $^3B \rightarrow {}^1A$ is increased from 800 to 2100 cm^{-1} (Figure 5a). Consequently, the UB3PW91/LANL2DZ calculation predicts that the symmetry of the T_1 state in $[Ru(bpy)_3]^{2+}$ is D_3 -like in vacuo or in less-polarizable media, whereas it was lowered to C_2 with a large dipole moment in polarizable media. In the DFT calculation, the critical *g* factor for the alternation between

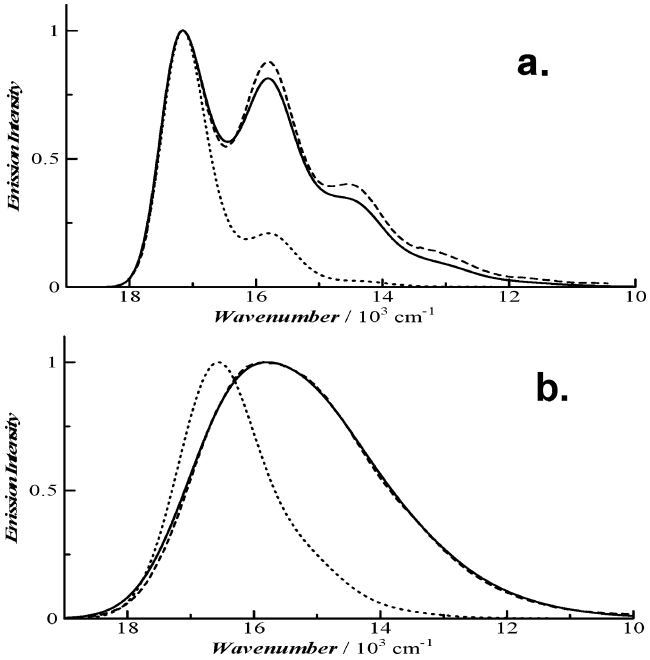

Figure 6. Experimental and calculated phosphorescence spectra for [Ru(bpy)$_3$]$^{2+}$. (a) Dashed line, observed in glassy butyronitrile at 77 K; solid line, calculated using S factors for the structure at $g = 3.6$, $\nu_{inh} = 550$ cm^{-1}, $\nu_{00} = 17.52 \times 10^3$ cm^{-1}, $T = 77$ K, and $\lambda_s = 0$. Dotted line, calculated using S factors for the structure of $^3A_2$, $\nu_{inh} = 600$ cm^{-1}, $\nu_{00} = 17.46 \times 10^3$ cm^{-1}, $T = 77$ K, and $\lambda_s = 0$. (b) Dashed line, observed in acetonitrile at 298 K; solid line, calculated using S factors for $g = 3.6$, $\nu_{inh} = 350$ cm^{-1}, $\nu_{00} = 17.37 \times 10^3$ cm^{-1}, $T = 298$ K, and $\lambda_s = 635$ cm^{-1}. Dotted line: calculated using S factors for $^3A_2$, $\nu_{inh} = 910$ cm^{-1}, $\nu_{00} = 16.94 \times 10^3$ cm^{-1}, $T = 298$ K, and $\lambda_s = 45$ cm^{-1}.

the D_3-like and C_2 structures was 2.0. However, the T_1 state obtained using another pure density functional of UPW91-PW91 was D_3-like even for g factors greater than 4.0, suggesting that the critical g factor tends to depend strongly on the density functional. Considering the empirical character of Beck's three parameters in eq 1, whether the T_1 state is D_3-like or C_2 should be determined with the help of spectroscopic data and not from the DFT calculation alone.

The next-lowest ^{3}A state has a dipole moment of 4.7 D under a wide range of the g factor. The direction of the vector was along the C_2 axis, opposite to that for ^{3}B, with 7.5 D, indicating that the excited electron is delocalized on two bpy ligands. As the delocalization decreases the distortion of the structure, the reorganization energy for the $^3A \rightarrow {}^1A$ was 1100 cm^{-1}, much less than that for localized ^{3}MLCT but slightly more than that for the fully delocalized one ($^3A_2$).

The phosphorescence spectrum of [Ru(bpy)$_3$]$^{2+}$ in a glass matrix exhibits a well-defined Franck−Condon progression with a spacing of ca. 1350 cm^{-1} (Figure 6a, dashed line). The emission spectrum simulated from the C_2 structure almost reproduces the progression (Figure 6a dashed line), whereas the vibronic satellite at around 15 800 cm^{-1} in the simulated spectrum for the D_3 structure is too weak. The simulation indicates that progression with a spacing of 1350 cm^{-1} resulted from the weighted average of several intraligand modes with 991 ($S = 0.163$), 1168 (0.055), 1168 (0.040), 1464 (0.237), 1465 (0.105), and 1534 cm^{-1} (0.131) (see the Supporting Information, Section B). In fluid solution, the emission spectrum was broad and red-shifted (~1300 cm^{-1}) compared to that at 77 K (Figure 6b, dashed line). The red shift of the emission spectrum is ascribed to solvation reorganization energy λ_s that resulted from the orientational polarization of the polar solvent. The λ_s value calculated using the PCM model (eq 9) was 635 cm^{-1} for the C_2 structure in acetonitrile and only 45 cm^{-1} for the D_3 structure. Simulation using these λ_s values revealed that the observed broad phosphorescence spectrum in fluid acetonitrile (Figure 6b, solid line) was consistent with the predicted spectrum for the polar T_1 state. Consequently, the theoretical analysis of the emission spectrum revealed that the phosphorescence in both a glass matrix and in fluid solution originated from the same C_2 structure with a considerable dipole moment of 7.5 D and a distorted structure with respect to that in the ground state ($\lambda_{vib} = 2100$ cm^{-1}).

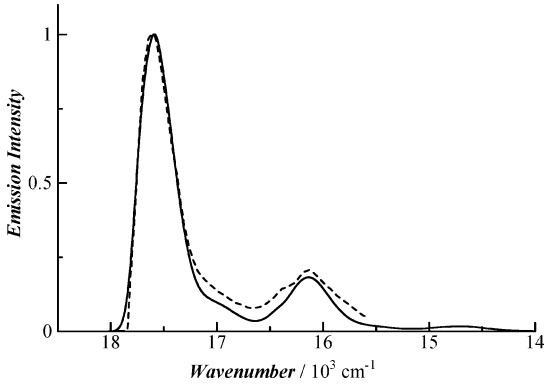

Figure 7. Experimental and calculated phosphorescence spectra for [Ru(bpy)$_3$]$^{2+}$. (a) Dashed line, observed in a [Ru(bpy)$_3$](PF$_6$)$_2$ single crystal at 2 K (ref 71) with $H = 6$ T; solid line, calculated using S factors for the structure of $^3A_2$. $\nu_{inh} = 180$ cm^{-1}, $\nu_{00} = 17.71 \times 10^3$ cm^{-1}, $T = 2$ K, and $\lambda_s = 0$.

The phosphorescence spectrum reported for neat crystals of PF_6 salt was also investigated because the emission spectra exhibited features quite different from those observed in solution or glassy matrix. Figure 7 shows the spectrum observed at 2 K in the [Ru(bpy)$_3$](PF$_6$)$_2$ single crystal in a high magnetic field of 6 T.[65] The strong magnetic field was found to increase the intensity of the phosphorescence at low temperature, and the enhancement is interpreted in terms of mixing between the lowest triplet sublevels and higher-lying sublevels with high radiative rates. The spectrum is, therefore, anticipated to have the minimum contribution of vibronic bands. It is noteworthy that the vibrational satellite at 16.1 $\times 10^3$ cm^{-1} is remarkably weak compared with that for the glassy matrix (Figure 6a). Such a pattern of vibrational progression is almost in agreement with that in the transition of $^3A_2 \rightarrow {}^1A_1$, which is calculated from the geometrical parameters obtained within the D_3 constraint. The weak vibrational satellites in the observed spectrum are consistent with negligible distortion of the structure of $^3A_2$ compared with the ground state; the largest changes in bond length are only 0.02 Å, and the vibrational reorganization energy is only 750 cm^{-1} for the phosphorescence, almost one-third of that for the localized ^{3}MLCT structure (2100 cm^{-1}). The good agreement between the simulated and observed spectra

(65) Krausz, E.; Riesen, H.; Rae, A. D. *Aust. J. Chem.* **1995**, *48*, 929.

indicates that the geometry of the phosphorescence state in the $[Ru(bpy)_3](PF_6)_2$ single crystal is almost the same as that for a delocalized ^{3}MLCT. The emission spectrum observed for $[Ru(bpy)_3](PF_6)_2$ at 5 K without a magnetic field is similar to that in Figure 7.[72] In the $[Ru(bpy)_3](PF_6)_2$ crystal, the $[Ru(bpy)_3]^{2+}$ molecule lies at a special position of C_3 symmetry, and the emission spectra observed in such a highly symmetric matrix probably exhibit features quite different from those observed in solution or glassy matrix. Emission spectra similar to that in Figure 7 are also observed for lower-symmetry hosts. The fast decay component in the emission spectrum for crystals doped into $[Zn(bpy)_3]SO_4$[73a] or $[Zn(bpy)_3](ClO_4)_2$[73b] and the spectrum observed at a higher temperature (20 K) in the doped perchlorate salt[73c,74a] show a rather weak sideband around 16×10^3 cm^{-1}.

Highly resolved luminescence spectra for $[Ru(bpy)_3]^{2+}$ were observed in a crystal doped into $[Zn(bpy)_3](ClO_4)_2$ at a very low temperature.[74−76] The most outstanding feature of the emission spectra is a very broad and intense phonon sideband appearing at around 250 cm^{-1}. In the highly resolved emission spectra for $[Rh(bpy)_3]^{3+}$ [70] and $[Os(bpy)_3]^{2+}$,[65] similar broad sidebands were also observed and assigned to lattice modes. The maxima of these sidebands, however, appeared at a much lower energy (50 cm^{-1}) than those of $[Ru(bpy)_3]^{2+}$. Thus, the unique feature of the strong phonon sideband in the highly resolved luminescence spectra in $[Ru(bpy)_3]^{2+}$ suggests a considerable contribution of low-frequency intramolecular vibrational modes with larger S factors. A simulation using the same parameters as those of the emission spectra in the glass matrix except for $\tilde{\nu}_{inh} = 4$ cm^{-1} and $T = 1.2$ K gave a spectrum quite different from the reported one (Figure 8a).[74−76] A remarkable difference between the simulated and experimental spectra is that the Franck−Condon progressions due to low-frequency modes were more striking in the simulated one. The progressions originate from twisting modes with larger S factors, 36.3 ($S = 1.54$), 40.6 (1.13), and 130.4 cm^{-1} (0.73), arising from the structural distortion associated with excitation localization. Because the frequencies of these modes are close to those of lattice modes, ∼100 cm^{-1},[69] these modes are likely to resonantly couple with the lattice modes, causing broadening of their frequencies. We then tried to simulate the spectrum provided that low-frequency modes less than 130 cm^{-1} were slightly broadened with fwhm = 25 cm^{-1} in a Gaussian distribution function. Surprisingly, the resulting spectrum shown in Figure 8b was very similar to that observed for $[Ru(bpy)_3]^{2+}$ doped into the $[Zn(bpy)_3](ClO_4)_2$ crystal.[74−76] The vibrational satellites characterizing the observed spectra are almost completely reproduced in the simulation: observed vibrational energies in cm^{-1} [26] (calculated) are 33 (35a_1,39e), 78 (81e), 110 (116e,124a_1), 158 (150a_1), 439 (435e), 477 (464e), 667 (650a_1), 767 (743a_1,-743e), 1015 (1005a_1), 1029 (991e), 1174 (1168a_1,e), 1325 (1301a_1,e), 1496 (1464e,1465a_1), 1559 (1534a_1,e), and 1569 (1579a_1,e). The intensity of the sideline at 477 cm^{-1} corresponding to the 464e mode is much stronger in the observed spectra than in the simulation of the vibrational structure ascribed to only Franck−Condon progression. In the case of ^{3}MLCT states, spin−orbit coupling of d electrons causes splitting of the lowest triplet state (zero-field splitting), and the state with the pure triplet characteristic is most stabilized.[12] Emission at a very low temperature is dominated by transition from the lowest sublevel with very small radiative probability and thus sidelines caused by vibrationally induced spin−orbit coupling tend to appear. Such vibronic coupling is probably responsible for the prominent satellite of the 477 cm^{-1} mode.

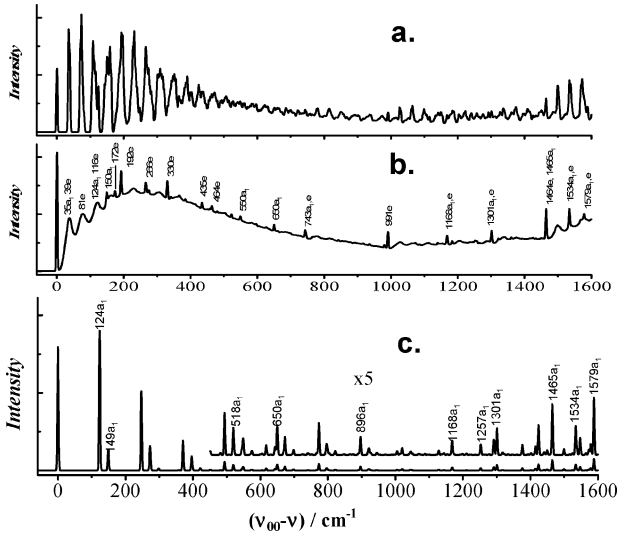

Figure 8. (a) Simulated highly resolved emission spectrum for $[Ru(bpy)_3]^{2+}$ using the same parameters as those of the solid line in Figure 6a except that $\tilde{\nu}_{inh} = 4$ cm^{-1} and $T = 1.2$ K. (b) Same as (a) but mode-specific broadening for low-frequency modes less than 130 cm^{-1} was assumed (fwhm = 25 cm^{-1}). (c) Simulated spectra using the $^3A_2$ structure with $\tilde{\nu}_{inh} = 4$ cm^{-1} and $T = 1.2$ K.

A highly resolved spectrum was simulated for the fully delocalized ^{3}MLCT (Figure 8c) for comparison. Because there is less contribution from low-frequency intramolecular vibrational modes, the spectrum shows only well-resolved satellites. It is obvious that the pattern of the vibrational satellites in the range 500−1600 cm^{-1} in the reported spectra closely resembles that in Figure 8b rather than that in Figure 8c. These results lead to the conclusion that the structure of the ^{3}MLCT in the doped crystals is identical to that in the fluid and in the glass matrix, i.e., a localized ^{3}MLCT. This

(66) (a) Rillema, D. P.; Jones, D. S. *J. Chem. Soc., Chem. Commun.* **1979**, 849. (b) Biner, M.; Bürgi, H.-B.; Ludi, A.; Röhr, C. *J. Am. Chem. Soc.* **1992**, *114*, 5197.
(67) (a) Richiter, M.; Scott, B.; Brewer, K. J.; Willett, R. D. *Acta Crystallogr., Sect. C* **1991**, *47*, 2443. (b) Constable, E. C.; Raithby, P. R.; Smit, D. N. *Polyhedron* **1989**, *8*, 367.
(68) Krausz, E.; Higgins, J.; Riesen, H. *Inorg. Chem.* **1993**, *32*, 4053.
(69) Yersin, H.; Braun, D. *Chem. Phys. Lett.* **1991**, *179*, 85.
(70) (a) Humbs, W.; Yersin, H. *Inorg. Chem.* **1996**, *35*, 2220. (b) Komada, Y.; Yamauchi, S.; Hirota, N. *J. Phys. Chem.* **1986**, *90*, 6425.
(71) Gallhuber, E.; Hensler, G.; Yersin, H. *J. Am. Chem. Soc.* **1987**, *109*, 4818.
(72) Hensler, G.; Gallhuber, E.; Yersin, H. *Inorg. Chim. Acta* **1986**, *113*, 91.
(73) (a) Ferguson, J.; Krausz, E. *Chem. Phys. Lett.* **1982**, *93*, 21. (b) Yersin, H.; Humbs, W.; Strasser, J. *Coord. Chem. Rev.* **1997**, *159*, 325. (c) Riesen, H.; Wallace, L.; Krausz, E. *Chem. Phys. Lett.* **1994**, *228*, 605.
(74) (a) Gallhuber, E.; Hensler, G.; Yersin, H. *Chem. Phys. Lett.* **1985**, *120*, 445. (b) Komada, Y.; Yamauchi, S.; Hirota, N. *J. Phys. Chem.* **1988**, *92*, 6511.
(75) Kato, M.; Yamauchi, S.; Hirota, N. *Chem. Phys. Lett.* **1989**, *157*, 543.
(76) Figure 19 in ref 26.

conclusion is, however, inconsistent with the small *S* factors of the internal ligand modes in the doped crystals. Yersin et al. reported that the largest *S* factors of the internal ligand modes are 0.1 for $[Ru(bpy)_3]^{2+}$,[69] much smaller than the value of 0.3 for a localized ^{3}LC in $[Rh(bpy)_3]^{3+}$.[70a] The calculated *S* factors for the C_2 structure are 0.11 for $1465a_1$, 0.24 for 1464e, 0.074 for $1534a_1$, and 0.13 for 1534e, whereas those for the D_3 structure are 0.12 for $1465a_1$ and 0.061 for $1534a_1$. Interestingly, the *S* factors for totally symmetric modes are almost constant, less than 0.12, regardless of whether ^{3}MLCT is delocalized or localized. The intensities of these satellites may not simply correspond to *S* factors when the line-widths of a_1 and e symmetric modes are not uniform. Long-range electrostatic coupling between the crystalline environment and the electric dipole moment induced by IR-active e modes might cause further inhomogeneous broadening.

(iii) $[Os(bpy)_3]^{2+}$. Solvation-induced polarization of the T_1 state occurs also for $[Os(bpy)_3]^{2+}$(Figure 6b). For $^3[Ru(bpy)_3]^{2+}$, because the change in state occurs suddenly, two structures are obtained as candidates for the T_1 state in the DFT calculation: D_3 (or D_3-like) and C_2 structures. On the other hand, for $^3[Os(bpy)_3]^{2+}$, the dipole moment in the T_1 state gradually changes from 0 D to 15 D, accompanied by an increase in the λ_{vib} value from 400 to 1000 cm^{-1}, at a *g* factor of 4.5−5.5, which allows for the presence of various structures depending on the degree of polarization. Nevertheless, by comparing the emission spectra simulated using the geometrical parameters obtained in the DFT calculations with the observed ones, we can choose structures suitable for $^3[Ru(bpy)_3]^{2+}$ and $^3[Os(bpy)_3]^{2+}$.

The observed phosphorescence spectrum for $[Os(bpy)_3]^{2+}$ in a butyronitrile glass at 77 K shows much weaker vibrational satellites than those for $[Ru(bpy)_3]^{2+}$(Figure 9a, solid line), suggesting a less-distorted structure in the T_1 state. The spectra simulated for the D_3-like T_1 structures with *g* factors less than 4 did not agree with the observed ones, because the intensity of the satellite around 12 800 cm^{-1} was too weak (Figure 9a, dashed line). The simulated spectrum corresponding to the structure with $g = 5.1$ or $g = 5.3$ is close to the observed one. The dipole moment of the T_1 state was 4.86 D and the λ_{vib} value was 1000 cm^{-1}, about half of those values for $^3[Ru(bpy)_3]^{2+}$. Therefore, a structure slightly deviated from D_3 symmetry seems to be responsible for the phosphorescence in a glass matrix. The slight deviation around the vibrational satellite at 12.8×10^3 cm^{-1} is probably due to multiple-state emissions from triplet sublevels split widely because of spin−orbit coupling of the 5d electron in Os(II). In fact, it is observed that the emission spectrum undergoes a substantial red shift and a decrease in its intensity in the PMM matrix as the temperature is lowered from 77 to 4.2 K. Therefore, accurate simulation of the emission spectra for the Os(II) compound requires the consideration of multiple emissions from thermally equilibrated triplet sublevels.

It is of great interest that the phosphorescence spectrum of $[Os(bpy)_3]^{2+}$ observed in fluid solution cannot be reproduced using the same *S* factors as those used for the simulation in a glass matrix, as shown in Figure 9b. The

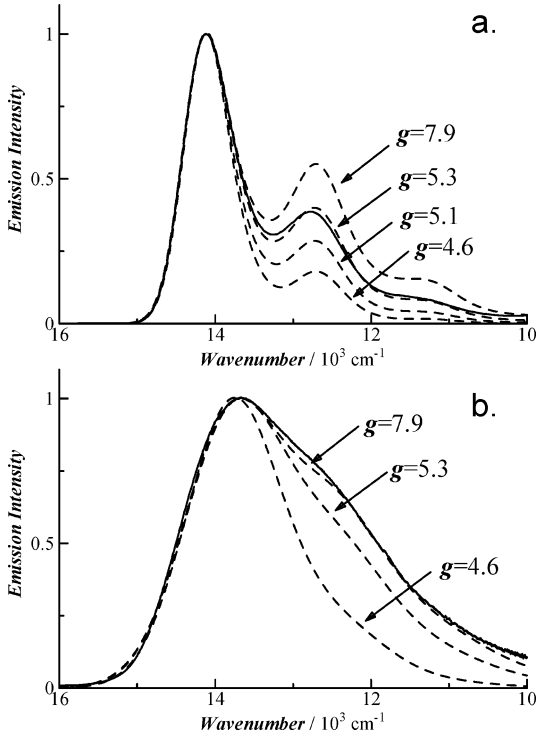

Figure 9. Experimental and calculated phosphorescence spectra for $[Os(bpy)_3]^{2+}$. (a) Solid line, observed in glassy butyronitrile at 77 K. Dashed lines: calculated using $T = 77$ K, $\lambda_s = 0$, and *S* factors for the structures at various *g* values. The other parameters are as follows. $g = 7.9$: $\nu_{inh} = 500$ cm^{-1}, $\nu_{00} = 14.38 \times 10^3$ cm^{-1}; $g = 5.3$: $\nu_{inh} = 530$ cm^{-1}, $\nu_{00} = 14.35 \times 10^3$ cm^{-1}; $g = 5.1$: $\nu_{inh} = 550$ cm^{-1}, $\nu_{00} = 14.30 \times 10^3$ cm^{-1}; $g = 4.6$: $\nu_{inh} = 550$ cm^{-1}, $\nu_{00} = 14.28 \times 10^3$ cm^{-1}. (b) Solid line, observed in dichloromethane at 298 K. Dashed lines: calculated using $T = 298$ K, and *S* factors for the structures at various *g* values. $g = 7.9$: $\nu_{inh} = 100$ cm^{-1}, $\lambda_s = 1000$, $\nu_{00} = 15.08 \times 10^3$ cm^{-1}; $g = 5.3$: $\nu_{inh} = 790$ cm^{-1}, $\lambda_s = 415$, $\nu_{00} = 14.42 \times 10^3$ cm^{-1}; $g = 4.6$: ν_{inh}=1200 cm^{-1}, $\lambda_s = 0$, $\nu_{00} = 13.92 \times 10^3$ cm^{-1}.

intensity of the sideband at around 12 500 cm^{-1} is stronger than the simulated value, indicating that the T_1 structure in dichloromethane is more distorted than that in glassy butyronitrile. Spectral fitting was achieved using the geometries obtained for $g = 8$, the properties of which were similar to those for $^3[Ru(bpy)_3]^{2+}$. Consequently, the spectrum simulation on the basis of the DFT geometries suggests that the degree of structural distortion of $^3[Os(bpy)_3]^{2+}$ varies with the dielectric constant of the medium. In a polarizable medium, the T_1 structure is rather distorted from D_3 symmetry, as is the case of $^3[Ru(bpy)_3]^{2+}$, whereas the degree of distortion falls considerably in a glass matrix, where orientational polarization is frozen.

Highly resolved emission spectra are also reported for $[Os(bpy)_3]^{2+}$ doped into $[Ru(bpy)_3](PF_6)_2$.[77] Because of the highly symmetric environment in the host crystal, the 0−0 transition band was not observed in the emission spectra at 1.2 K, whereas the spectra exhibit many vibrational satellites that are not assigned as Raman bands, indicating that the phosphorescence from the lowest triplet sublevel is strongly

(77) (a) Yersin, H.; Gallhuber, E.; Hensler, G. *Chem. Phys. Lett.* **1987**, *140*, 157. (b) Yersin, H.; Huber, P.; Braun, D. *J. Phys. Chem.* **1990**, *94*, 3560. (c) Huber, H.; Yersin, H. *J. Phys. Chem.* **1993**, *97*, 12705. (d) Braun, D.; Hensler, G.; Gallhuber, E.; Yersin, H. *J. Phys. Chem.* **1991**, *95*, 1067.

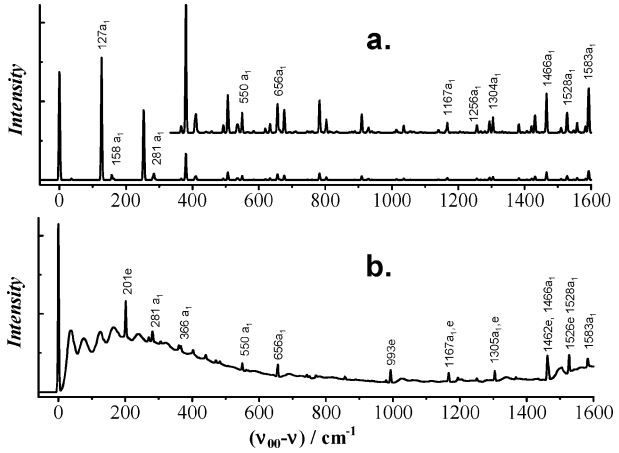

Figure 10. (a) Simulated highly resolved emission spectra for $[Os(bpy)_3]^{2+}$ using the *S* factor for $^3A_2$ and $\tilde{\nu}_{inh} = 4$ cm^{-1} and $T = 1.2$ K (b) Same as (a) but using the geometries for ^3B ($g = 7.9$). Broadening of low-frequency modes less than 130 cm^{-1} was assumed (fwhm = 25 cm^{-1}).

dipole-forbidden.[77] Thus, simulation of the phosphorescence spectra needs a large number of vibronic couplings with asymmetric vibrational modes. Applying a strong magnetic field to the crystals, however, remarkably enhanced the intensity of the 0−0 transition band as well as totally symmetric vibrational satellites.[77] The vibrational satellites induced by the magnetic field almost agreed with those in the spectrum simulated for the D_3 structure (Figure 10a) except for the intensity at 127 cm^{-1}; the observed[77] (calcd) bands are 155 (127), 175 (158), 296 (281), 675 (656), 1048 (1013), 1172 (1167), 1270 (1256), 1320 (1304), 1491 (1466), 1552 (1527), and 1610 (1583) cm^{-1}. The difference is that the contribution of the 127 cm^{-1} mode is somewhat larger in the simulation compared with the observed one. This mode is a twisting motion of the bpy ligand around the C(2)−C(2′) bond, and the calculated large *S* factor (1.2) is ascribed to the change in the dihedral angle (ca. 3.5°) of pyridine rings in the T_1 state. The spectrum was simulated also for the C_2 structure, making the same assumptions as those for $[Ru(bpy)_3]^{2+}$ for comparison. The spectrum features both a broad band due to lattice-mode-coupled low-frequency modes and additional satellites of e modes, such as 201, 993, 1167, 1305, 1262, and 1526 cm^{-1}, which were not seen in the observed spectrum (Figure 10b). Therefore, the phosphorescence spectra are derived from delocalized ^{3}MLCT.

Deuteration Shift of Electronic Origins

To confirm the electronic configuration of the T_1 structures in the Rh(III) and Ru(II) compounds, we calculated the electronic origins (0−0 transition energies) for fully or partially deuterated compounds.[78] Deuteration-induced shifts of origin have been observed for many organic and metal compounds.[69] The shift is ascribed to the deuteration-induced change in zero-point energy (ZPE) of the ground and excited states. The deuteration shifts of ZPE are usually very small, several per centimeter. The extent of the deuteration shift and/or pattern of the shift upon partial deuteration gives crucial evidence for the localization of the excited electron. The ZPE levels calculated for the T_1 states in $[Rh(bpy)_3]^{3+}$ and $[Ru(bpy)_3]^{2+}$ were lower by 600−1000 cm^{-1} compared to the ground state, as shown in Table 2, originating from a softening of the force constants in the excited states. The calculation for $[Rh(bpy)_3]^{3+}$ predicts the blue shift of the origin to 69 cm^{-1} upon the per-deuteration of the compound, consistent with the observed blue shift of 61 cm^{-1} for $[Rh(bpy)_3]^{3+}$ in $[Zn(bpy)_3](ClO_4)_2$.[70a] The amount of blue shift for $[Ru(bpy)_3]^{2+}$ depended on the electronic configuration of ^{3}MLCT. The per-deuteration-induced blue shift was calculated to be 35 cm^{-1} for the localized ^{3}MLCT(^{3}B), whereas it was 28 cm^{-1} for the fully delocalized ^{3}MLCT-($^3A_2$); however, the pattern of the shift for the partial deuteration of bpy was quite different in the two cases. In the former case, the partial replacement of bpy-h_8 by bpy-d_8 causes the appearance of two origins corresponding to the localized ^{3}MLCT involving bpy-h_8 and bpy-d_8 at around those for $[Ru(bpy\text{-}h_8)_3]^{2+}$ and $[Ru(bpy\text{-}d_8)_3]^{2+}$. On the other hand, the partial replacement yields only the shift of the origin in the latter case. The per-deuteration-induced blue shifts of 37 and 41 cm^{-1} observed for $[Ru(bpy)_3]^{2+}$ in $[Ru(bpy)_3](ClO_4)_2$[25,27] are closer to those (35 cm^{-1}) for the localized ^{3}MLCT; furthermore, the appearance of two origins, and the pattern of their energetic shifts upon partial replacement of bpy-h_8 by bpy-d_8, observed by Riesen et al. was in excellent agreement with those calculated for the localized ^{3}MLCT in Table 2.[25] The appearance of two origins for the partially deuterated complexes have been claimed by Yersin et al. They observed only one origin for the $x = 1$ system at the same position as that for $[Ru(bpy\text{-}h_8)_3]^{2+}$ and asserted that the emitting state is a delocalized ^{3}MLCT. However, such a negligible deuteration shift is inconsistent with the gradual shift predicted for the fully delocalized ^{3}MLCT ($^3A_2$) (Table 2). Moreover, Riesen et al. have pointed out that the intensities of excitation to the bpy-d_8 ligand decreased when luminescence was monitored at the lower-energy side of inhomogeneously broadened bpy-h_8 emission of $[Ru(bpy\text{-}h_8)_2(bpy\text{-}d_8)]^{2+}$, because the emission of the complexes with the bpy-d_8 ligand in the crystallographically unique position

(78) As the DFT calculation tends to slightly overestimate the force constants, an empirical scaling factor is often used to correct vibrational frequency. As shown in the text, there is a slight deviation between the observed vibrational frequencies observed in the highly resolved emission spectra and the calculated ones. The average ratio of the observed against the calculated in 35 modes was 1.045, suggesting that the reported scaling factor of 0.9521 for the B3PW91/LANL2DZ level causes over-correction for these complexes and no scaling factor might be needed. The error of 5% in the correction gives rise to systematic errors in the calculated frequency and also in the deuteration shift of the electronic origin. The difference in ZPE between the S_0 and T_1 states is obtained by $\Delta ZPE = ZPE(T_1) - ZPE(S_0) = \sum_{i=1}^{3N-6} 1/2\ \hbar\omega_i(T_1) - \sum_{i=1}^{3N-6} 1/2\ \hbar\omega_i(S_0)$, where the vibrational frequency is the square root of the force constant over reduced mass, $\omega = \sqrt{k/\mu}$. The 5% error in the scaling factor corresponds to an error of 5×10^4 cm^{-1} of the total ZPE, which is about 1×10^6 cm^{-1} in the case of the tris-bpy metal complexes. Because structural changes between the ground and the excited states are very small in these compounds, the ΔZPE values are only about −1000 cm^{-1}, as shown in Table 2, which is only 0.1% of the total ZPE, and its error is at most 50 cm^{-1}. The deuteration shift of the electronic origin is then calculated from the difference between ΔZPE for the protonated and deuterated complexes. The shift results from the difference in reduced mass, i.e., $\omega_D/\omega_H = \sqrt{\mu_H/\mu_D}$. (D shift) = ΔZPE(d) − ΔZPE(h). As the deuteration effects of ΔZPE are a few percent of the value for the ruthenium complexes, the 5% error in the correction is considered to result in an error of 1−2 cm^{-1} in the deuteration shift of electronic origin.

Table 2. Calculated Deuterium Effects on Zero-Point Energy (ZPE) and the Electronic Origin in $[Rh(bpy)_3]^{3+}$ and $[Ru(bpy)_3]^{2+}$ with Localized (^3B), Partially Delocalized (^3A), and Fully Delocalized ^3MLCT ($^3A_2$)

compds	difference in ZPE (cm^{-1})[a]	deuteration-induced blue shift (cm^{-1})[78] calcd	obsd
$[Rh(bpy\text{-}h_8)_{3-x}(bpy\text{-}d_8)_x]^{3+}$ (^3B, C_2)[b]			
$x = 0$	−984		
$x = 3$	−915	69	61[d]
$[Ru(bpy\text{-}h_8)_{3-x}(bpy\text{-}d_8)_x]^{2+}$ (^3B, C_2)[b,c]			
$x = 0$	−622(h)	-	
$x = 1$	−574(d), −629(h)	48(d), −7(h)	0[e], 50[f], −4.7[f],
$x = 2$	−581(d), −635(h)	41(d), −13(h)	47[f], −8.5[f]
$x = 3$	−587(d)	35(d)	37[e],41[f]
$[Ru(bpy\text{-}h_8)_{3-x}(bpy\text{-}d_8)_x]^{2+}$ (^3A, C_2)[c]			
$x = 0$	−794(hh)		
$x = 1$	−775(hd), −801(hh)	19(hd), −7(hh)	
$x = 2$	−756(dd), −782(hd)	38(dd), 12(hd)	
$x = 3$	−763(dd)	31(dd)	
$[Ru(bpy\text{-}h_8)_{3-x}(bpy\text{-}d_8)_x]^{2+}$ ($^3A_2$, D_3)			
$x = 0$	−1021		
$x = 1$	−1012	10	
$x = 2$	−1002	19	
$x = 3$	−993	29	(32)[g]

[a] ZPE(ES) − ZPE(GS). [b] Calculated with $g = 3.6$ for T_1. [c] "h" and "d" mean that the promoted electron is promoted to bpy-h_8 and bpy-d_8, respectively. [d] From ref 70a. [e] From ref 25. [f] From ref 26. [g] Value for $[Os(bpy)_3]^{2+}$ in $[Ru(bpy)_3](PF_6)_2$[77c, 79].

is slightly lower in energy than that for the complexes with the other orientation.[21]

Deuteration effects were also calculated for ^3A of $[Ru(bpy)_3]^{2+}$, the second-lowest excited state for comparison. In the excited state, the promoted electron is delocalized over two bpy ligands and two origins appear for the $x = 1$ and $x = 2$ systems, just like in the localized one. The energy difference between the two origins is about half that for the localized one.

The blue shift of 28 cm^{-1} for the delocalized ^3MLCT is close to the value of 32 cm^{-1} observed for the per-deuteration of $[Os(bpy)_3]^{2+}$ doped in $[Ru(bpy)_3](PF_6)_2$.[77c,79] However, the shift of the origin upon partial deuteration is found to be 10 cm^{-1} ($x = 2$), inconsistent with that calculated for the delocalized ^3MLCT, a gradual shift by 9 cm^{-1} per one bpy-d_8. Riesen et al. showed that partial deuteration localizes the ^3MLCT of $[Os(bpy)_3]^{2+}$ doped in $[Ru(bpy)_3](PF_6)_2$.[79] This DFT calculation suggests the presence of slightly polarized ^3MLCT states with less-distorted structures (those calculated for a g factor less than 4).

In the case of $[Os(bpy)_3]^{2+}$ doped in $[Ru(bpy)_3](ClO_4)_2$, the interaction between the ^3MLCT states involving crystallographically equivalent ligands is larger than in the PF_6 salt. Two sets of the origins are observed, as is the case for $[Ru(bpy)_3]^{2+}$ in the same host. The observed deuteration shifts are 13 and −5 cm^{-1} for $x = 1$, 35 and 10 cm^{-1} for $x = 2$, and 30 cm^{-1} for $x = 3$,[80] for which the pattern is quite close to that predicted for ^3A of $[Ru(bpy)_3]^{2+}$. This result suggests that the promoted electron is delocalized over two bpy ligands, although we have still not found the ^3MLCT geometry that can reproduce the highly resolved emission spectra in the perchlorate salt.

0−0 Transition Energy of Phosphorescence. Fitting of the observed emission spectra using simulated spectra taking into consideration the effects of both the Franck−Condon progression and solvent polarization allows for the determination of accurate 0−0 transition energies even from broad emission spectra obtained in solution or in glass matrix. Table 3 summarizes the 0−0 transition energies determined for the phosphorescence examined. The similarity in the 0−0 energies of the bpy compounds of Zn(II), Rh(III), and Ir(III) ions indicates that the phosphorescence states are characterized by $^3\pi\pi^*$ of bpy. For $[Ru(bpy)_3]^{2+}$, the 0−0 energies are not so different in various media. Although the 0−0 energy in solution is 0.2×10^3 cm^{-1} higher than that in glass matrix and comparable to the energy in the solid states, it is anticipated to be lower than that in glassy or solid states, because the polar ^3MLCT state is stabilized by solvation. A slight overestimation of the solvent reorganization energy using the PCM solvation model might cause a positive error in the 0−0 transition energy.

Table 3. The 0−0 Transition Energies of Phosphorescence for the Tris-Chelate Metal Compounds Determined by Spectral Fitting

compds	0−0 transition energy[a] (10^3 cm^{-1})
$[Zn(bpy)_3]^{2+}$	23.15
$[Rh(bpy)_3]^{3+}$	22.25
$[Ir(bpy)_3]^{3+}$	22.21
$[Ru(bpy)_3]^{2+}$	17.52
sol[b]	17.7
neat cryst. PF_6	17.71
doped crystal [c]	17.68
$[Os(bpy)_3]^{2+}$	14.30
sol[d]	14.1
doped crystal [e]	14.495

[a] Values given are for in a glass matrix unless stated. [b] In acetonitrile at 298 K. [c] Doped into $[Zn(bpy)_3](ClO_4)_2$. [d] In dichloromethane at 298 K. [e] Doped into $[Ru(bpy)_3](PF_6)_2$.

Discussion

Geometries of Emitting States. Computational chemistry now provides accurate information on the geometrical and electronic structures of molecules without empirical parameters. Even for molecules containing heavy atoms, current DFT calculations predict geometrical parameters within 1%

(79) Riesen, H.; Wallace, L.; Krausz, E. *J. Chem. Phys.* **1995**, *102*, 4823.
(80) Riesen, H.; Krausz, E. *Chem. Phys. Lett.* **1996**, *260*, 130.

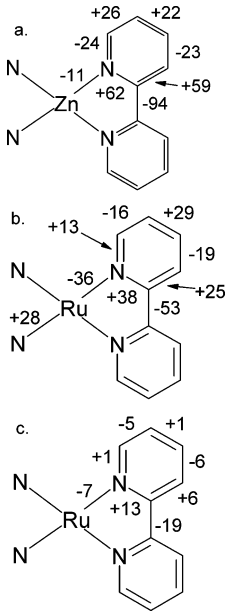

Figure 11. Changes in bond lengths (in mÅ) in T_1 geometry with respect to the S_0 state for (a) $[Zn(bpy)_3]^{2+}$, (b) $[Ru(bpy)_3]^{2+}$ as ^3B with $g = 3.6$, and (c) $[Ru(bpy)_3]^{2+}$ as $^3A_2$.

error and provide reliable assignment of observed vibrational spectra.[81] For some valence excited-states of coordination compounds, however, the electronic structures calculated for the lowest excited state occasionally depend on the quantum chemical model employed because many excited states with different electronic configurations are usually present in a narrow energy region. For such complicated cases, as demonstrated in this work, the vibrational structures of emission spectra of transition metal compounds can be used to determine the correct geometries of the emitting states.

In this calculation of vibrational structures for large sized molecules such as transition metal compounds, a rather simplified model is adopted for the vibronic states involved in emission. The normal vibrational analysis on the basis of DFT is carried out with a crude adiabatic approximation around the minimum potential-energy surface, and the harmonic oscillator approximation is used for evaluation of the overlap integral of vibrational wave functions (or Huang−Rhys factors). Any rotation of normal coordinates or change in force constants in the excited state is also ignored in the simulations. These effects influence the intensity of vibrational satellites; however, even for the ^{3}LC phosphorescence spectra with rather complicated vibrational structures, the simulated spectra are in excellent agreement with those observed, which indicates that errors arising from this approximation are not so large for bpy compounds. The calculated geometrical changes associated with the emission of $^3[Zn(bpy)_3]^{2+}$ (^{3}LC), $^3[Ru(bpy)_3]^{2+}$ (localized ^{3}MLCT), and $^3[Ru(bpy)_3]^{2+}$ (delocalized ^{3}MLCT) are shown in Figure 11a−c, respectively.

The phosphorescence state of $[Zn(bpy)_3]^{2+}$ is $^3\pi\pi^*$ of bpy, in which the electron is promoted from a bonding π orbital to an antibonding π^* orbital in a single bpy. The highest occupied π orbital and LUMO in bpy are depicted in Figure 12. Because most of the C−C bonds have an opposite phase between the highest occupied π orbital and LUMO, both the removal and addition of an electron cause considerable changes in the geometry of bpy. In particular, the interpyridine C−C bond length is shortened by 94 mÅ (Figure 11a). Such structural distortions are responsible for the large λ_{vib} value of 4000 cm^{-1}.

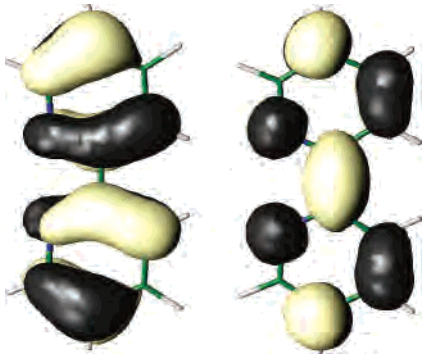

Figure 12. The highest occupied π orbital (left) and LUMO (right) of bpy.

This analysis of the emission spectrum revealed that the phosphorescence of $[Ru(bpy)_3]^{2+}$ in both a glass matrix and in fluid solution originated from the same C_2 structure with a dipole moment of 7.5 D and a distorted structure (λ_{vib} = 2100 cm^{-1}). In the localized ^{3}MLCT state, one of the bpy ligands is greatly distorted as shown in Figure 11b, whereas the geometries of the other bpy ligands remain almost unchanged. The vibrational reorganization energy of 2100 cm^{-1} for the phosphorescence process is almost half that of $^3[Zn(bpy)_3]^{2+}$ (4000 cm^{-1}). The reason for the smaller vibrational reorganization energy in ^{3}MLCT is that electrons are promoted from d orbitals with a nonbonding character, whereas electrons in bonding π orbitals of ligands are promoted for ^{3}LC. Changes in bond length for the localized ^{3}MLCT are about half of those for ^{3}LC, as seen in panels a and b of Figure 11. The Ru−N bond of the bpy, where the excited electron is localized, decreases by 36 mÅ, whereas those at the trans positions increase.

As shown in Figure 7, the emission spectra for the $[Ru(bpy)_3](PF_6)_2$ single crystal exhibit very weak vibrational satellites compared with the spectra in the glass matrix in Figure 6a. The spectrum simulation indicates that the geometry of the phosphorescence state is almost the same as that for the delocalized ^{3}MLCT with negligible distortion, as shown in Figure 11c; the largest change in bond length is only 0.02 Å and the vibrational reorganization energy is only 750 cm^{-1} for phosphorescence, about one-third of that for the localized ^{3}MLCT structure (2100 cm^{-1}).

Is the Emitting State of $[Ru(bpy)_3]^{2+}$ Localized or Delocalized? The electronic configurations of MLCT states in $[Ru(bpy)_3]^{2+}$ and $[Os(bpy)_3]^{2+}$ with a D_3 structure are interpreted in terms of two trigonal field-splitting parameters.[7,8,10] Three degenerated dπ (T_{2g}) orbitals split into dπ(e) and dπ(a_1), and the energy difference between them is denoted by the quantity Δ, which is positive if dπ(a_1) lies higher than dπ(e). The energy of the π^* orbitals of three bpy is also split into π^*(e) and π^*(a_2) by Γ, which is positive

(81) Scott, A. P.; Radom, L. *J. Phys. Chem.* **1996**, *100*, 16502.

if $\pi^*(e)$ lies higher than $\pi^*(a_2)$. The electronic configuration of the lowest excited state depends on these trigonal splitting parameters: large values of Δ and Γ decrease the energy of $^3A_2$ ($d\pi(a_1) \rightarrow \pi^*(a_2)$), whereas a decrease in Γ lowers the ^3E ($d\pi(a_1) \rightarrow \pi^*(e)$) state. In addition, a further decrease in Δ values stabilizes the $^3A_1$ ($d\pi(e) \rightarrow \pi^*(e)$) state. Whereas the electronic configurations of both $^3A_2$ and $^3A_1$ are delocalized ^{3}MLCT, the doubly degenerated ^3E tends to couple with asymmetric vibrations (e mode) and the symmetry of the structure is lowered because of the Jahn−Teller effect.[82] On the other hand, when the energy level of ^3E against $^3A_2$ (or $^3A_1$) is higher than the Jahn−Teller relaxation energy, the ^{3}MLCT should be delocalized. One of the factors determining the magnitude of Δ and Γ is the degree of Ru $\rightarrow$ bpy π-back-donation: with increasing orbital mixing between $d\pi(e)$ and $\pi^*(e)$, $d\pi(e)$ stabilizes, whereas $\pi^*(e)$ destabilizes. Because $d\pi(a_1)$ does not mix with $\pi^*(a_2)$, a strong π-back-donation results in the increase in both Δ and Γ values and thereby stabilizes $^3A_2$ with a delocalized ^{3}MLCT configuration.[83] The extent of the Ru $\rightarrow$ bpy π-back-donation increases with a decreasing energy gap between $d\pi(e)$ and $\pi^*(e)$ and with an increasing principal quantum number of d orbitals. Therefore, the stabilization of $^3A_2$ against ^3E is expected for $[Os(bpy)_3]^{2+}$ than for $[Ru(bpy)_3]^{2+}$, which supports our assessment that the structure of $^3[Os(bpy)_3]^{2+}$ is almost D_3, whereas that of $^3[Ru(bpy)_3]^{2+}$ is C_2 in glassy butyronitrile. Direct calculation of the trigonal splitting parameters or the energy difference between $^3A_2$ (or $^3A_1$) and ^3E in ^{3}MLCT electronic configurations is not easy and has not been reported so far. The Δ and Γ values seem to depend on the degree of electron correlation and/or electron-exchange interaction, which is one of the reasons for the strong dependence of the lowest-excited-state configuration on the calculation levels, such as density functionals.

Simulation of the spectra for $[Ru(bpy)_3]^{2+}$ both in fluid solution and in glass matrix supports the assessment that phosphorescence originates from localized ^{3}MLCT, consistent with the results of resonance Raman and transient infrared measurements.[38−40] Stabilization of the polar localized ^{3}MLCT can be rationalized because of the polarizability of solvent. On the other hand, assessment of the emission in single crystals is not so straightforward. The features of highly resolved vibrational structures of $[Ru(bpy)_3]^{2+}$ doped into $[Zn(bpy)_3](ClO_4)_2$ seem to be well-reproduced by simulations on the basis of the geometry of localized ^{3}MLCT. The predicted deuteration shifts of the electronic origins in $[Ru(bpy\text{-}h_8)_{3-x}(bpy\text{-}d_8)_x]^{2+}$ are in excellent agreement with those observed by Riesen et al. The zero-field splittings observed in the perchlorate salts are very close to those in glass matrix[84] and, moreover, those predicted for localized ^{3}MLCT geometry by a recent quantum-mechanical calculation including spin−orbit coupling.[12] These results strongly support the assessment that the phosphorescence state in the doped crystals is localized ^{3}MLCT. The symmetry of the site available for guest molecules in the $[Zn(bpy)_3](ClO_4)_2$ crystal is C_2; two ligands are crystallographically equivalent, whereas the crystallographically unique ligand lies on the C_2 axis. The MLCT transition to the unique ligand is estimated to be several hundred wave numbers higher in energy compared with transition to the crystallographically equivalent ligand.[25b] Such reduction of symmetry of the environment probably stabilizes the ^{3}MLCT with distorted C_2 symmetry. Although most of the observed features are consistent with predictions made on the basis of the localized model, an apparent disagreement is found in the vibrational structures for partially deuterated compounds in the range of high-frequency modes around 1500 cm^{-1}. Figure 13 shows simulated vibrational structures ranging from 1000 to 1600 cm^{-1} for $[Ru(bpy\text{-}h_8)_{3-x}(bpy\text{-}d_8)_x]^{2+}$. The spectrum for the $x = 0$ system is very close to the observed one (Figure 19 in ref 26, Figure 13 in ref 24a). Emission spectra involving bpy-d_8 in the $x = 2$ and $x = 3$ systems are also close to those reported by Riesen et al., except for the 1080 cm^{-1} mode.[24] The intensity of this mode seems to be sensitive to sample conditions, because its intensity is weak in the spectrum reported by another group.[27] For emission involving bpy-h_8 in the $x = 1$ and $x = 2$ systems, the observed spectra exhibit not only the bpy-h_8 modes of 1492 and 1559 cm^{-1} but also the bpy-d_8 modes of 1429 and 1523 cm^{-1}, whereas only the bpy-h_8 modes appear in the simulated ones, as shown in Figure 13. The simultaneous appearance of both bpy-d_8 and bpy-h_8 modes is in dispute because it is likely to support the delocalized model. For this phenomenon, Riesen et al. explained it in terms of electronic interaction between the reduced bpy-h_8 and unreduced bpy-d_8 through the metal center. Although such electrostatic interaction is taken into account in this DFT calculation, nevertheless, the geometries of the unreduced bpy in localized ^{3}MLCT are almost the same as those in the ground state. Therefore, either the interring stretching modes or ring-breathing modes of the unreduced bpy are Franck−Condon inactive in the radiative

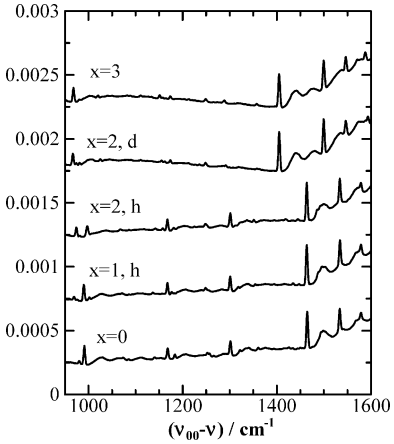

Figure 13. Simulated highly resolved emission spectra of localized ^{3}MLCT (^3B) state in $[Ru(bpy\text{-}h_8)_{3-x}(bpy\text{-}d_8)_x]^{2+}$ in the region of ligand-localized vibrational modes using the same parameters as those in Figure 8b.

(82) Ignoring the changes in the force constant between the excited and ground states, we approximate the Jahn−Teller distortion energy to form ^3B as the vibrational reorganization energy of e-modes in the $^3B \rightarrow {}^1A_1$ transition. For $[Ru(bpy)_3]^{2+}$, the sum of the reorganization energy calculated from eq 5 is 1400 cm^{-1}.

(83) Yersin, H.; Braun, D. *Coord. Chem. Rev.* **1991**, *111*, 39.

(84) (a) Harrigan, R. W.; Hager, G. D.; Crosby, G. A. *Chem. Phys. Lett.* **1973**, *21*, 487. (b) Hager, G. D.; Crosby, G. A. *J. Am. Chem. Soc.* **1975**, *97*, 7031.

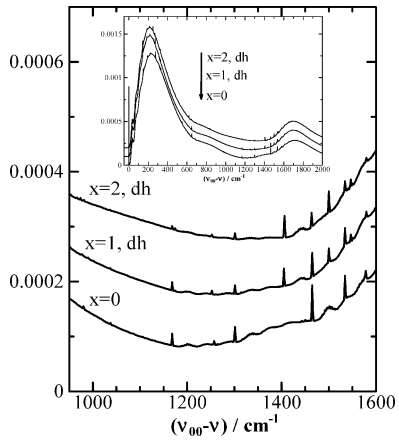

Figure 14. Simulated spectra of the partially delocalized ^{3}MLCT (^{3}A) state in $[Ru(bpy\text{-}h_8)_{3-x}(bpy\text{-}d_8)_x]^{2+}$ ($x = 0, 1, 2$) in the region of ligand-localized vibrational modes using the same parameters as those in Figure 8b except $\nu_{inh} = 2$ cm^{-1}. Insert: the whole simulated spectra.

transition from localized ^{3}MLCT. As described in the previous section, the changes in C−C bond lengths of bpy are caused by the promotion of an electron into the π^* orbital and, therefore, the appearance of both the bpy-d_8 and bpy-h_8 modes with equal intensity implies that the promoted electron stays on both ligands for almost the same period of time.

The appearance of vibrational satellites of both bpy ligands suggests that the emitting state is not ^{3}B but ^{3}A, in which the promoted electron is delocalized over two bpy ligands. The simulated spectra of the emission from ^{3}A are shown in Figure 14. Whereas for the $x = 0$ system, the vibrational structure in the region from 1200 to 1600 cm^{-1} is similar to that of the localized ^{3}MLCT shown in Figure 13, both the bpy-d_8 (1406, 1500, and 1547 cm^{-1}) and bpy-h_8 (1464, 1534, and 1539 cm^{-1}) modes appear in the spectra for the $x = 1$ and $x = 2$ systems. The patterns of the four vibrational satellites resemble those observed; however, the idea that the emission in the doped crystal comes from the partially delocalized ^{3}MLCT is readily excluded. In the spectrum for the $x = 0$ system shown in Figure 14, the satellites at 742 and 991 cm^{-1} are very weak, whereas those at 650 and 1168 cm^{-1} are relatively strong compared with the spectra shown in Figures 8b and 13. The satellites of 991 and 742 cm^{-1} are ring-breathing vibrational modes with e symmetry. These features are not seen in the observed spectra.[24,27] Moreover, the trend of the deuterium shifts of the electronic origins in Table 2 is different from the observed trend.[25,26]

The failure to simulate the vibrational satellites for the partially deuterated compounds doped in $[Zn(bpy)_3](ClO_4)_2$ is probably ascribed to the environmental model used in the calculation of the structure of localized ^{3}MLCT. Because of the local electric field in the crystalline environment, the transition energy to the two ^{3}MLCT states involving crystallographically equivalent ligands is lower than that involving the crystallographically unique ligand. The direction of the electric field is opposite to that of the reaction field in the Onsager model used for the geometry calculation. For technical reasons, the geometry calculation under the applied electric field simulating the crystalline environment is currently difficult to perform. Probably, the interaction between two energetically equivalent ^{3}MLCT states should be taken into account to understand the behavior of the localized ^{3}MLCT in this particular environment.

The behaviors of $[Os(bpy)_3]^{2+}$ in $[Zn(bpy)_3](ClO_4)_2$ provide useful information about the effects of interaction between two localized ^{3}MLCT states on the photophysical properties, because Davydov splitting due to exciton coupling is observed: 79 cm^{-1} for sublevel I and 163 cm^{-1} for sublevel II.[85] Interestingly, the behavior of $[Os(bpy)_3]^{2+}$ is very similar to that of $[Ru(bpy)_3]^{2+}$: the simultaneous appearance of the vibrational modes of crystallographically equivalent bpy-d_8 and bpy-h_8,[85] and observation of two sets of origins in the partially deuterated complexes.[86] This similarity implies that the exciton coupling between two localized ^{3}MLCT states is also the origin of the simultaneous appearance of the bpy modes for $[Ru(bpy)_3]^{2+}$. This idea is, however, inconsistent with the fact that the excitation exchange interaction in the ruthenium complex is too small (<0.5 cm^{-1})[73c] to interpret the simultaneous appearance with almost similar intensities of bpy-d_8 and bpy-h_8 despite the large difference of zero-point energy between the ^{3}MLCT states (40 cm^{-1}).

For intramolecular energy transfer between two localized ^{3}MLCT states, the potential-energy curve as a function of the total reaction coordinate is symmetrically W-shaped. The energy barrier between two potential wells is roughly given by $S\hbar\omega$. The S factor can be approximated by the sum of the S factors for e symmetric vibrational modes in the transition of ^{3}MLCT → GS by ignoring the difference in force constants between the two states. From the S factors for the emission of localized ^{3}MLCT (see Table B3 in the Supporting Information), it is found that the asymmetric distortion of the geometry occurs for mainly two effective reaction coordinates: distortion of the bpy frame with high-frequency vibrational modes (Q_H) of 1000−1550 cm^{-1} and a sum of the S_H factors of only about 0.75, and the torsion of the coordinate structure with a considerably low frequency of 30−330 cm^{-1} (Q_L), of which the total S_L factor is about 2. Such considerably large displacement with the low-frequency mode is responsible for the origin of the broad background, as described in the simulation of the highly resolved spectrum. Therefore, the interaction between the ^{3}MLCT states should be considered for both the Q_L and Q_H coordinates. As these modes are remarkably different in frequency, the motion on the Q_H coordinate is thought to be almost independent of that on the Q_L coordinate. The zero-point energy of the low-frequency mode $1/2\hbar\omega_L$ is much lower than $S_L\hbar\omega_L$, which is the lowest energy barrier between the ^{3}MLCT states for the Q_L coordinate, and the adiabatic approximation holds for this mode. On the other hand, the zero-point energy of the high vibrational mode $1/2\hbar\omega_H$ is similar to the energy barrier $S_H\hbar\omega_H$ in the Q_H coordinate,

(85) Huber, P.; Yersin, H. *J. Phys. Chem.* **1993**, *97*, 12705.
(86) Riesen, H.; Wallace, L.; Krausz, E. *Mol. Phys.* **1996**, *87*, 1299. For the partially deuterated $[Os(bpy)_3]^{2+}$, two sets of origins are observed because of different orientations in the lattice. The behaviors of the origins, e.g., in narrowed excitation spectra, are different from those observed for $[Ru(bpy)_3]^{2+}$.

and therefore the adiabatic approximation is broken. As a result, vibronic coupling between two ^{3}MLCT states for the Q_H coordinate causes mixing between their vibrational wave functions. This is probably the reason for the simultaneous appearance of the C−C stretching mode of crystallographically equivalent bpy ligands. Even in this situation, the exciton coupling between the localized vibronic states is still very small because of the considerably large distortion of the Q_L coordinate. Although deuteration shifts of the origins under such mode-specific vibronic coupling are difficult to predict accurately, they should be between those for ^{3}MLCT (^{3}B) and ^{3}MLCT (^{3}A) in Table 2.

Yamauchi et. al found that the vibrational structures of emission from the triplet sublevel II are different from that for the sublevel I.[74b] The difference is more obvious in the time-resolved emission spectra observed by Yersin et al. (Figure 9 in ref 73b). The luminescence from $[Ru(bpy)_3]^{2+}$ showed non-single-exponential decay when the origin of sublevel III was excited at a temperature below 2 K in the doped perchlorate salt. The fast component, with a lifetime of 220 ns, originates from sublevel II, whereas the slow component, with a lifetime of 230 μs, is assigned to the lowest sublevel, sublevel I. It is of great interest that the fast component shows a vibrational structure different from that of the slow one; the peak intensity of broad background around 1400 cm^{-1} in the fast component is considerably weak, and the satellites at 1029 and 767 cm^{-1} disappeared. These differences in vibrational structure were interpreted in terms of Herzberg−Teller vibronic coupling; however, the features of the vibrational structure in the high-frequency region of the emission of sublevel II resemble those in the spectrum simulated using a structure in which ^{3}MLCT is delocalized over two Ru-bpy subunits (Figure 14). This similarity suggests that two bpy frames are simultaneously distorted at sublevel II; however, it is obvious that the exciton coupling between two ^{3}MLCT vibronic states dose not occur, because the resonance splitting of sublevel II is quite small (<0.5 cm^{-1}). Also, the deuteration shift of the origins for sublevel II is almost equivalent to that for sublevel I. Therefore, these features should be interpreted by strong vibronic coupling for high-frequency modes in sublevel II, not by exciton coupling. Whereas for sublevel I, the amplitude of the vibrational wave function of the Q_H mode under vibronic coupling still has two maxima at each localized ^{3}MLCT states, it is maximized at the middle of the Q_H coordinate in sublevel II because of stronger vibronic coupling. Such stronger coupling in sublevel II might be due to differences in spin function between these sublevels.[86]

The results of simulating the unresolved spectrum in the neat crystal of $[Ru(bpy)_3](PF_6)_2$ are also inconsistent with the assignment on the basis of the deuterium effects of their electronic origins. Whereas the unresolved spectrum was well-reproduced using the fully delocalized ^{3}MLCT geometry in this work, two sets of origins were observed in the excitation spectra of the lowest-energy site in the $[Ru(bpy\text{-}h_8)(bpy\text{-}d_2)_2](PF_6)_2$.[24c] The behaviors of the deuteration shifts of the origins are the same as those for the doped perchlorate salts. Furthermore, the zero-field splittings determined from the electronic origins in the emission spectrum of the highest-energy site are almost identical to those in the doped crystal.[72] Therefore, the origins in the neat crystal are thought to originate from the localized ^{3}MLCT; however, the unresolved spectra observed in the PF_6 salts with a high magnetic field[71] and the short-lived emission component in the sulfate or perchlorate salt[73] exhibit remarkably weak vibrational sideband of around 1400 cm^{-1}, indicating that the emission originates from ^{3}MLCT geometry with less distortion of the bpy frame. This feature is obviously different from that observed in the doped perchlorate salt and in the glass matrix.

The peculiar feature in vibrational structure of the unresolved emission of the PF_6 salt might be interpreted in terms of stronger vibronic coupling, as discussed for the emission from sublevel II in the perchlorate salt. Unfortunately, the highly resolved vibrational structure of the PF_6 salt is observed only in the low-frequency region (<200 cm^{-1}), so that the further information on the geometry of bpy cannot be obtained at this stage.

Alternatively, the unresolved emission might originate from the ^{3}MLCT geometry that is different from that for the highly resolved emission of the perchlorate salt, because some of the photophysical properties obtained for the unresolved emission appear to be different from those for the electronic origins. It is reported that the radiative rate of the PF_6 salt is much lower than that for perchlorate salt,[87] which suggests that the lowest excited state belong to D_3 point group. In addition, the zero-field splitting obtained from the temperature dependence of the decay rates of unresolved emission is different from the splitting of the electronic origins,[88,89] although the analysis may be disturbed by phase transition. These phenomena should be interpreted in terms of dynamic Jahn−Teller effects.[90] Because of excess kinetic energy in e mode vibrations, the localized ^{3}MLCT states formed by the static Jahn−Teller effect are coupled dynamically beyond the energy barrier and unresolved emission originates from the resulting potential curve with the minimum being the averaged geometry.

In the $^3\pi\pi^*$ emission involving bpy-h_8 for $[Rh(bpy\text{-}h_8)_2(bpy\text{-}d_8)]^{3+}$ doped in $[Zn(bpy)_3](ClO_4)_2$ crystal, the bpy-d_8 modes are absent,[70a] which is in contrast to the case for $[Ru(bpy)_3]^{2+}$ or $[Os(bpy)_3]^{2+}$. Electronic interaction between the localized $^3\pi\pi^*$ states in $[Rh(bpy)_3]^{3+}$ requires electronic coupling not only between π^* orbitals but also between π orbitals of the ligands, whereas the interaction of the ^{3}MLCT states originates simply from the resonance between π^* orbitals of ligands through π-back-donation of ruthenium 4d orbitals. Consequently, the electronic coupling between the localized $^3\pi\pi^*$ states is expected to be rather weaker than that for ^{3}MLCT. The time-dependent DFT calculation gave 4.0 cm^{-1} as the electronic coupling between the localized

(87) Yersin, H.; Hensler, G.; Gallhuber, E. *Inorg. Chim. Acta* **1987**, *132*, 187.
(88) Yersin, H.; Gallhuber, E. *J. Am. Chem. Soc.* **1984**, *106*, 6582.
(89) Islam, A.; Ikeda, N.; Nozaki, K.; Ohno, T. *Chem. Phys. Lett.* **1996**, *263*, 209.
(90) (a) Canton, S. E.; Yencha, A. J.; Kukk, E.; Bozek, J. D.; Lopes, M. C. A.; Snell, G.; Berrah, N. *Phys. Rev. Lett.* **2002**, *89*, 045502. (b) Manini, N.; Tosatti, E. *Phys. Rev. Lett.* **2003**, *90*, 249601.

$^3\pi\pi^*$ states, two orders lower than for ^{3}MLCT in [Ru(bpy)$_3$]$^{2+}$(310 cm^{-1}) and in [Os(bpy)$_3$]$^{2+}$ (800 cm^{-1}).[91] Furthermore, the barrier between the localized $^3\pi\pi^*$ states for high-frequency modes should be much higher in energy than that for [Ru(bpy)$_3$]$^{2+}$ because of larger changes of the one bpy frame in excited-state geometry (Figure 11). As a result, the vibronic coupling between the localized $^3\pi\pi^*$ states in [Rh(bpy)$_3$]$^{3+}$ is much less important compared with [Ru(bpy)$_3$]$^{2+}$ and thus the behaviors of the ^{3}LC state are well-described in terms of the localized state under the crude adiabatic approximation.

This theoretical investigation indicates that the promoted electron of ^{3}MLCT in the Os(II) tris-chelate compounds tends to be delocalized compared with that in the Ru(II) compound. The trend is probably ascribable to the stronger π-back-donation of 5d electrons, which increases the trigonal field splitting between the energies of three π^* orbitals on ligands. TDDFT calculation for [Os(bpy)$_3$]$^{2+}$ gave the interaction between the localized ^{3}MLCT states as 800 cm^{-1},[91] two times greater than for [Ru(bpy)$_3$]$^{2+}$. It is of great interest that the phosphorescence spectrum of [Os(bpy)$_3$]$^{2+}$ observed in fluid solution cannot be reproduced using the same *S* factors as those used for simulation in a glass matrix, as shown in Figure 9b. The total width of the wide band is larger than the simulated value, indicating that the T_1 structure in dichloromethane is more distorted than that in glassy butyronitrile. Spectral fitting was achieved using the geometries obtained for $g = 8$, the properties of which are similar to those for ^{3}[Ru(bpy)$_3$]$^{2+}$. These results seem consistent with those of two-mode Franck−Condon analysis of emission spectra reported by Meyer et al.; the *S* factors obtained from the phosphorescence spectra of Os(II) diimine compounds, including [Os(bpy)$_3$]$^{2+}$, increased with increasing temperature.[92] Spectrum simulation on the basis of the DFT geometries supports these observations: the degree of the structural distortion of ^{3}[Os(bpy)$_3$]$^{2+}$ varies with the dielectric constant of the medium. In a polarizable medium, the T_1 structure is rather distorted from D_3 symmetry, as is the case of ^{3}[Ru(bpy)$_3$]$^{2+}$, whereas the degree of distortion falls considerably in a glass matrix, where orientational polarization is frozen. Variations in delocalization are also suggested in the PF_6 salt of [Os(bpy)$_3$]$^{2+}$. The origin upon partial deuteration is inconsistent with that calculated for the delocalized ^{3}MLCT, a gradual shift of 9 cm^{-1} per one bpy-d$_8$. ^{3}MLCT with an electronic structure distorted slightly from D_3 would be involved in [Os(bpy-h$_8$)$_{3-x}$(bpy-d$_8$)$_x$]$^{2+}$, $x = 1$ or $x = 2$.[79]

(91) Electronic coupling between two localized states is estimated from the excitation energies of the states in which the excited states are delocalized over two ligands with C_2 symmetry. For [Ru(bpy)$_3$]$^{2+}$ at the ^{3}A geometry where the promoted electron is delocalized over two ligands, the lowest state is ^{3}MLCT, in which the electron is promoted from the highest dπ orbital to the MO formed from the in-phase combination of LUMOs of two bpy ligands; the second-lowest state involves the MO formed from their out-of-phase combination. Thus, the energy difference between two states is approximately equal to twice the electronic resonance energy between the LUMOs, which was calculated as 620 cm^{-1} by time-dependent DFT at the B3PW91/LANL2DZ level. Consequently, electronic coupling between two localized ^{3}MLCT states is determined to be 310 cm^{-1}. Analogous with [Ru(bpy)$_3$]$^{2+}$, the geometry of a partially delocalized ^{3}MLCT was also obtained for [Os(bpy)$_3$]$^{2+}$. The TDDFT calculation of the geometry indicates that electronic interaction between localized ^{3}MLCT is 800 cm^{-1}. For the T_1 geometry of [Rh(bpy)$_3$]$^{3+}$ with C_2 symmetry, T_1 is the localized $^3\pi\pi^*$ state of the crystallographically unique bpy, whereas both T_2 and T_3 are in a delocalized $^3\pi\pi^*$ state over two equivalent ligands. The difference in excitation energy between T_2 and T_3 was calculated as being 8.0 cm^{-1}, which can be ascribed to electronic coupling between the localized $^3\pi\pi^*$ states.

(92) Lumpkin, R. S.; Meyer, T. J. *J. Phys. Chem.* **1986**, *90*, 5307.

Summary

The phosphorescence spectra of typical tris-chelate 2,2′-bipyridine metal compounds, [M(bpy)$_3$]$^{n+}$, were simulated on the basis of DFT calculations. It is revealed that the DFT calculation for the excited states can provide geometrical parameters that reproduce observed vibrational structures. The ordering of excited states in transition metal compounds very often depends on the density functional used for the calculation, especially for ^{3}MLCT, which may be caused by the incomplete description of long-range interaction in current density functionals. It is demonstrated that the combination of quantum chemical calculations with spectroscopic data is helpful in evaluating the consistency between the structure obtained by theoretical calculation and that responsible for spectroscopic data.

The simulations of phosphorescence spectra of the Zn(II), Rh(III), and Ir(III) compounds confirmed that the emission originated from localized ^{3}LC with C_2 symmetry and considerably distorted geometries.

The spectra observed for [Ru(bpy)$_3$]$^{2+}$ both in fluid and in the glass matrix are in good agreement with simulations on the basis of localized ^{3}MLCT. The highly resolved phosphorescence spectrum of [Ru(bpy)$_3$]$^{2+}$ in the doped [Zn(bpy)$_3$](ClO$_4$)$_2$ crystal was reproduced from the structure of localized ^{3}MLCT. The deuteration effects of the electronic origins are also in excellent agreement with the frequency calculation for localized ^{3}MLCT. On the other hand, the vibrational structures calculated for ^{3}MLCT involving bpy-h$_8$ in [Ru(bpy-h$_8$)$_{3-x}$(bpy-d$_8$)$_x$]$^{2+}$ ($x = 1,2$) show no contribution of bpy-d$_8$ modes, inconsistent with the observations. For the unresolved emission spectrum observed in a neat crystal of [Ru(bpy)$_3$](PF$_6$)$_2$, simulation of the whole spectrum indicated that the emitting state originated from delocalized ^{3}MLCT, contradictory to the assignments of the localized ^{3}MLCT on the basis of the deuterium shift of the electronic origins. The discrepancy between the simulated and observed patterns of the satellites of high-frequency bpy modes is probably ascribed to vibronic coupling between localized ^{3}MLCT states because the energy barrier of the high-frequency mode is close to its zero-point vibrational energy.

The degree of localization in [Os(bpy)$_3$]$^{2+}$ seems to vary depending on electrostatic interaction with the environment. The emission spectra observed in fluid solution are due to localized ^{3}MLCT, whereas in a glass matrix, phosphorescence comes from slightly localized ^{3}MLCT. On the other

hand, emission spectra in the PF_6 salt at 1.2 K exhibit features characteristic of delocalized ^{3}MLCT.

The results of this work suggest that the simple harmonic oscillator model in a single well is too simple to interpret these complicated aspects of ^{3}MLCT consistently. A more-sophisticated model including vibronic coupling among the degenerate Jahn−Teller states is necessary to fully understand the photophysical behavior of ^{3}MLCT.

Acknowledgment. K.N. gratefully acknowledges Monkasho for a Grant-in-Aid for Scientific Research (14540515 and 16550056).

Supporting Information Available: Listing of Cartesian coordinates and Huang−Rhys factors used for spectrum simulation. This material is available free of charge via the Internet at http://pubs.acs.org.

IC052068R